Marangoni instability in the linear Jeffreys fluid with a deformable surface

Ramkarn Patne,[1,2] Yehuda Agnon,[1] and Alexander Oron[2,*]

[1]*Faculty of Civil and Environmental Engineering, Technion-Israel Institute of Technology, Haifa 3200003 Israel*

[2]*Faculty of Mechanical Engineering, Technion-Israel Institute of Technology, Haifa 3200003 Israel*

(Received 26 February 2020; accepted 30 July 2020; published 19 August 2020)

Viscoelastic polymer films are present in numerous industrial applications such as in paint coatings, lubricants, and optoelectronics which involve a large variation in temperatures. The present study deals with the general linear stability analysis (GLSA) of a Jeffreys viscoelastic fluid layer having a deformable free surface deposited on a perfectly conducting slippery plate. Variation in temperature results in variation in surface tension thereby inducing Marangoni stresses leading, under certain conditions, to the emergence of instability of the quiescent, heat-conducting base state which may be either stationary or oscillatory. Accounting for the deformability of the free surface of the layer, the GLSA reveals the existence of the long-wavelength Marangoni instability absent in the previous studies that assumed a nondeformable free surface. The analysis reveals a strong effect of variation in the capillary number, Ca, on the stationary mode, whereas the oscillatory mode is moderately affected. The critical parameters for the stationary mode remain unaffected by variation in the Prandtl number, Pr, and the dimensionless relaxation L_1 and retardation L_2 parameters; however, their impact on the oscillatory modes is significant. Variation in the Biot number, Bi, has a stabilizing effect on the system. Variation in the Bond number, Bo, is found to strongly influence the long-wave regime of the stationary mode, but it does not influence the short-wave regime of the stationary mode and oscillatory modes. Variation in the slip coefficient leads to a moderate increase in Ma_c in the case of the stationary mode, whereas in the case of the oscillatory mode variation of both Ma_c and k_c is nonmonotonic. The energy balance analysis suggests that viscoelasticity of the fluid is responsible for the emergence of oscillatory instability. Our analysis reveals the existence of a wide parameter range where oscillatory modes determine the stability properties of the system. This result emphasizes that neglecting viscoelasticity of the fluid may lead to significant errors when the dynamics of a viscoelastic fluid is investigated. The present study further demonstrates that even for a highly elastic fluid, the interface deformability prevails and promotes the long-wave stationary instability at the expense of the oscillatory instability.

DOI: 10.1103/PhysRevFluids.5.084005

I. INTRODUCTION

Layers of soft matter and their stability is a subject of prime scientific and technological interest. The dynamics of thin liquid layers [1–3] is important to a wide variety of applications and contexts including paint coatings, plane wing deicing, and mucus blockage of lung airways. Generation of waves on film interfaces with small characteristic thicknesses may also contribute to the development of both miniaturized and microgravity heat and mass transfer technology. Polymer

*Corresponding author: meroron@technion.ac.il

thin films are ubiquitous in many applications such as microfluidics, functional coatings, lubricants, sensors and actuators, optoelectronics, and biotechnology. Singer [4] reviewed thermocapillary approaches to polymer patterning and emphasized that only since the early 2010s have these methods been developed and applied. Furthermore, the advantages of the thermocapillary techniques over other approaches to patterning assure that their applications will continue to expand and develop.

The general linear stability analysis (GLSA) of thermocapillary instability in a layer of a Newtonian fluid has been investigated already over several decades [5,6]. It was first studied theoretically by Pearson [7], who showed the emergence of an instability as a consequence of the surface-tension dependence on the temperature at the layer interface. The analysis of Pearson [7] showed that the cellular patterns observed by Bénard [8] in his pioneering studies are the result of thermocapillary or Marangoni instability. Scriven and Sternling [9], Smith [10], and Davis and Homsy [11] extended the study of Pearson [7] for a liquid layer with a flat interface to the system with a free deformable surface. Here a deformable surface refers to the liquid-gas interface with a finite surface tension whose presence allows its deformation in response among other factors to the tangential stresses arising due to surface-tension gradients referred to below as Marangoni stresses. Their analysis revealed a strong effect of the decrease in surface tension on the instability which is due to temperature variation along the interface. The Marangoni instability in a layer of Newtonian fluid was always found to be stationary, either short wave or long wave, until recently, when oscillatory instability, both long wave and short wave, was discovered in films [12,13] and layers [14].

Viscoelasticity of liquids has been extensively discussed in a variety of major aspects and models [15–17] among other properties of polymeric liquids. Various models of viscoelasticity constitute a significant technical complication over standard challenges encountered in dealing with Newtonian liquids. Some of the models such as those by Maxwell and Jeffreys [15–17] containing only linear terms are suitable for linearized studies involving a quiescent base state, whereas a comprehensive study of nonlinear dynamics requires more involved nonlinear models, such as the Oldroyd-B model [15]. As explained in Sec. II, in the present study, the *linear Jeffreys model* is employed. Here, the word "linear" is used to emphasize that only linear terms are present in the Jeffreys model.

The GLSA of Marangoni instability of viscoelastic layers was first carried out [18] for both Maxwell and Jeffreys [17] models of viscoelasticity under assumption that the liquid-gas interface is flat. While the Newtonian liquid layers with a temperature-independent density exhibit mostly stationary Marangoni instability, the viscoelasticity introduces novel effects so that both stationary and oscillatory instabilities are possible depending on the viscoelastic relaxation and retardation times. Here the terms stationary and oscillatory instabilities refer to the cases when the leading eigenvalue has a zero real part with a zero or nonzero imaginary part, respectively. The topic was further developed and extended to the cases of a coupled Rayleigh-Marangoni instability [19–21], a layer of a liquid with temperature-dependent viscosity [22], and a layer on a thick substrate [23]. A nonrobustness of a Maxwell-fluid model for the problem of Marangoni instability in a viscoelastic layer was discussed by Wilson [24]. In all these papers, both stationary and oscillatory types of instability were found. Coupled Rayleigh-Marangoni convection in thin polymeric layers was experimentally studied and hexagonal patterns were observed [25]. Various applications in polymeric liquids involving thermal effects and thermocapillarity in small scales were demonstrated experimentally [25–27].

It is interesting to note that the experiments with polymer layers [25] heated at the substrate side showed the emergence of hexagonal patterns akin to those emerging in a layer of a Newtonian liquid [28,29]. In the backdrop of these experiments, it is essential to understand the origin of the instability modes in order to unravel the experimentally observed patterns.

The previous studies [18–22,24] of the thermocapillary instability exhibited by viscoelastic fluids considered a nondeformable free surface. However, for the fluids with a moderate surface tension or in the case of a sufficiently high differential heating there exists a significant surface deformation eventually leading to the modification in the emerging instability. The coupled Rayleigh-Marangoni convection in a layer of a viscoelastic fluid with a deformable interface and heated from below was

also addressed in several papers [30–33]. Chiang [30] developed a numerical method to solve linear eigenvalue problems and applied it briefly to the linear stability analysis of the Marangoni instability in a layer of a Maxwell liquid.

Ramkissoon *et al.* [31] and Comissiong *et al.* [32] were the first to address the coupled Bénard-Marangoni instability in a layer of a linear Jeffreys liquid with a *deformable* interface. The governing equations employed in their studies were the Boussinesq equations whose main assumption for their validity is that

$$\alpha \Delta T \ll 1, \tag{1}$$

where α is the coefficient of volumetric thermal expansion and ΔT is the temperature difference across the layer. Velarde *et al.* [34] discuss in detail the issue of validity of the Boussinesq approximation in general and the criterion for its validity, in particular. Equation (1) can transformed in the form

$$\mathrm{Ra} \equiv \frac{g\alpha \Delta T d^3}{\nu\kappa} \ll \mathrm{Ga} \equiv \frac{gd^3}{\nu\kappa} = \frac{\mathrm{Bo}}{\mathrm{Ca}}, \tag{2}$$

where Ra, Bo, Ca, and Ga are, respectively, the Rayleigh, Bond, and capillary numbers, defined below in Eq. (9), and the modified Galileo number. The Galileo number, defined in the study of Ramkissoon *et al.* [31] and denoted there by G, is related to the modified Galileo number Ga via $\mathrm{Ga} = G\sigma$, where σ is the Prandtl number in their notation, which recasts Eq. (2) to the form

$$\mathrm{Ra} \ll G\sigma. \tag{3}$$

It is easy to see that most of the results [31] do not satisfy the validity criterion Eq. (3) around the criticality representing the parameter range of importance.

Another serious shortcoming of the theory presented there, which is again related to the use of the Boussinesq equations, is an inclusion of the interfacial deformation representing a non-Boussinesqian effect into these equations. An account and a detailed discussion of various incorrect results arising from this combination can be found in Velarde *et al.* [34]. Some of the examples of these incorrect results discussed there are contained in Benguria and Depassier [35], Perez-Garcia and Carneiro [36], and many others. Apart from the fact that a pure Marangoni instability was not addressed [31] at all and the results were presented only for a given ratio between the Marangoni and Rayleigh numbers, another inconsistency there [31] is associated with an assumption of $1/\mathrm{Ca} = 0$, which makes the upper bound in Eq. (3) vanish given the fact the Bond number is bounded, e.g., for water layers of thickness of 1 mm, the Bond number is $O(0.1)$. The assumption of $1/\mathrm{Ca} = 0$ implies a zero surface tension, i.e., an infinitely deformable interface. However, the interface of a liquid layer with an immiscible outer fluid has a finite surface tension which renders the assumption mentioned above to be unphysical. The other paper [32] follows the same pattern adding to the scope of Ref. [31] internal heat generation.

There is a growing practical and theoretical interest in extending our understanding of the coupled Bénard-Marangoni (also referred to as Rayleigh-Bénard-Marangoni) instability to the wide range of parameters that is covered by a non-Boussinesq theory. Such an extension is also consistent with the inclusion of the interfacial deformation which is on par with other non-Boussinesqian effects neglected in the Boussinesq approximation. A recent paper [37] highlights the importance of non-Boussinesq effects in Bénard-Marangoni convection in a Newtonian liquid layer with a deformable surface, demonstrating clear quantitative and qualitative differences in comparison to a Boussinesq-based theory. In particular, they found that at small values of Galileo number G, and when deformation of the free surface is important, there are significant differences in stability behavior as compared to results obtained using the Boussinesq approximation.

Sarma and Mondal [33] considered the pure Marangoni instability in a layer of a Maxwell liquid with a deformable interface subjected to a constant temperature gradient imposed at the substrate. They found that a stationary short-wave mode along with both short-wave and long-wave oscillatory

instability modes emerge. In most cases discussed there, the instability sets in as a competition between the oscillatory modes.

The present work aims at filling the gap in the current knowledge and at a further understanding of the role of the fluid viscoelasticity in a layer of a linear Jeffreys fluid with a *deformable* surface and its effect on the pure Marangoni instability by revisiting the problem in its consistent mathematical and physical context. The forthcoming linear stability analysis reveals the parametric regimes where stationary, either short wave or *genuinely* long wave, and oscillatory instability emerge. The effect of slippage at the substrate on the instability properties is also discussed. This analysis may be potentially helpful in understanding observed patterns in future relevant experiments in viscoelastic liquid layers.

The rest of the paper is arranged as follows. In Sec. II, the problem is formulated, governing linearized equations and boundary conditions are derived, and the corresponding Orr-Sommerfeld problem is posed for the perturbed state by introduction of normal modes. The results obtained from the linear stability analysis via numerical solution of the Orr-Sommerfeld eigenvalue problem are presented and discussed in Sec. III. The salient conclusions of the present study are summarized in Sec. IV. The details of numerical methodology used here are addressed in Appendix.

II. PROBLEM FORMULATION

We consider a layer of an incompressible viscoelastic liquid of a mean thickness d and of an infinite lateral extent with temperature-independent viscosity μ, density ρ, kinematic viscosity ν, and thermal diffusivity κ deposited on a horizontal planar substrate. The layer is bounded by the ambient inert gas phase at the liquid-gas interface which is assumed to be a free deformable surface with the surface tension σ^*. The planar substrate and the ambient gas phase are assumed to be held at the respective uniform temperatures T_0^* and T_∞^*, such that the temperature difference between these is $\Delta T^* = T_0^* - T_\infty^* > 0$.

The coordinate system used here is Cartesian with the axes x^* and y^* located in the substrate plane, whereas the axis z^* is normal to the substrate and directed into the liquid layer with the reference point $z^* = 0$ located on the substrate plane. Surface tension σ^* of the fluid is assumed to be temperature dependent,

$$\sigma^* = \sigma_0^* - \gamma^*(T^* - T_0^*), \tag{4}$$

where $\gamma^* = -\frac{d\sigma^*}{dT^*} > 0$ and σ_0^* is the surface tension of the fluid at the reference temperature of the lower plate T_0^*. In what follows, the asterisk denotes dimensional variables, whereas their counterparts without asterisk decoration express their dimensionless variants.

The length, velocity, time, and temperature are nondimensionalized by $d, \kappa/d, d^2/\kappa$, and βd, respectively, where $\beta = -\frac{d\bar{T}^*}{dz^*}$ and an overbar denotes a base-state quantity. Furthermore, pressure and stresses are nondimensionalized by $\mu\kappa/d^2$. We denote the dimensionless fluid velocity field as $\mathbf{v} = (v_x, v_y, v_z)$ with v_i being the velocity components in the direction i, $i = x, y, z$.

The dimensionless continuity and momentum conservation Cauchy equations are

$$\nabla \cdot \mathbf{v} = 0, \tag{5}$$

$$\frac{1}{\mathrm{Pr}}\left[\frac{\partial \mathbf{v}}{\partial t} + (\mathbf{v}\cdot\nabla)\mathbf{v}\right] = -\nabla p - G\mathrm{Pr}\nabla z + \nabla\cdot\boldsymbol{\tau}, \tag{6}$$

where $\mathrm{Pr} = \frac{\mu}{\rho\kappa}$ is the Prandtl number, $G = \frac{gd^3}{\nu^2}$ is the Galileo number, $\nabla = (\frac{\partial}{\partial x}, \frac{\partial}{\partial y}, \frac{\partial}{\partial z})$ is the gradient operator, p is the pressure, and $\boldsymbol{\tau}$ is the stress field. The dimensionless heat advection- diffusion equation is

$$\frac{\partial T}{\partial t} + (\mathbf{v}\cdot\nabla)\,T = \nabla^2 T, \tag{6a}$$

where $\nabla^2 \equiv \frac{\partial^2}{\partial x^2} + \frac{\partial^2}{\partial y^2} + \frac{\partial^2}{\partial z^2}$ is the Laplacian operator.

To describe the rheological behavior of the Jeffreys viscoelastic fluid, three types of models, viz., corotational Jeffreys, upper-convected Jeffreys, or lower-convected Jeffreys models [15], can be utilized. The difference in these models is in the way the time derivative in the linear Jeffreys model is made objective or frame invariant. The terms arising due to the frame-invariant time derivative are nonlinear for all the three models. In the linear stability analysis of the present problem, due to the fact that the base state is quiescent, any nonlinear term in the constitutive equation will not contribute. Thus, for the perturbed state, the linearized about the quiescent base-state corotational Jeffreys, upper-convected Jeffreys, or lower-convected Jeffreys models will result in the same equations as the linear Jeffreys model. Consequently, in the present work, the linear Jeffreys model is used to describe the fluid viscoelasticity.

The dimensionless linear Jeffreys rheological equation reads [15–17]

$$\left[1 + L_1 \frac{\partial}{\partial t}\right] \boldsymbol{\tau} = \left[1 + L_2 \frac{\partial}{\partial t}\right] (\nabla \mathbf{v} + \nabla \mathbf{v}^T), \tag{7}$$

where $L_1 = \frac{\lambda_1^* \kappa}{d^2}$ and $L_2 = \frac{\lambda_2^* \kappa}{d^2}$ with λ_1^* and λ_2^* representing dimensional relaxation and retardation times, respectively.

The governing equations (5)–(7) are subjected to the following boundary conditions. Assuming extension of the Navier slip model for slippage [38], impermeability and a constant specified temperature at the solid substrate $z = 0$ yields

$$v_x = \zeta \tau_{xz}; \quad v_y = 0; \quad v_z = 0; \quad T = T_0. \tag{8a}$$

At the deformable gas-liquid interface $z = \xi(x, y, t)$, the boundary conditions are the kinematic boundary condition, the tangential and normal components of the stress balance [36], and the continuity of the heat flux, respectively,

$$\frac{\partial \xi}{\partial t} + \mathbf{v}_\perp \cdot \nabla \xi = v_z, \tag{8b}$$

$$\mathbf{t} \cdot \boldsymbol{\tau} \cdot \mathbf{n} = -\mathrm{Ma} \nabla T \cdot \mathbf{t}, \tag{8c}$$

$$-p + \mathbf{n} \cdot \boldsymbol{\tau} \cdot \mathbf{n} = -\frac{1}{\mathrm{Ca}} (\nabla \cdot \mathbf{n}) - \frac{\mathrm{Bo}}{\mathrm{Ca}} \xi, \tag{8d}$$

$$\nabla T \cdot \mathbf{n} = -\mathrm{Bi}(T - T_\infty), \tag{8e}$$

where

$$\mathrm{Ma} = \frac{\gamma \beta d^2}{\mu \kappa}, \quad \mathrm{Bo} = \frac{\rho g d^2}{\bar{\sigma}^*}, \quad \mathrm{Bi} = \frac{q d}{k_{\mathrm{th}}}, \quad \mathrm{Ca} = \frac{\mu \kappa}{\bar{\sigma}^* d} \tag{9}$$

are, respectively, the Marangoni, Bond, Biot, and capillary numbers and $\mathrm{Bo} = G\mathrm{Ca}$. Here q, $\bar{\sigma}^*$, g, and k_{th} are the coefficient of thermal convection at the free surface, surface tension evaluated at the free surface temperature, gravity acceleration, and thermal conductivity of the fluid. The vectors $\mathbf{t} = \mathbf{e_x} + \frac{\partial \xi}{\partial x} \mathbf{e_z}$ and $\mathbf{n} = -\frac{\partial \xi}{\partial x} \mathbf{e_x} + \mathbf{e_z}$ represent the unit tangent and normal vectors to the free surface, respectively. Also, the vector $\mathbf{v}_\perp$ is the two-dimensional part of vector $\mathbf{v}$, $\mathbf{v}_\perp = (v_x, v_y)$.

The two terms in the boundary condition Eq. (8c) represent the contributions of deviatoric viscous and viscoelastic components to the tangential stress at the layer interface and of the Marangoni stress. The terms in the boundary condition Eq. (8d) from the left to the right represent the contributions of pressure, deviatoric viscous and viscoelastic components to the normal stress balance at the layer interface, and the effects of capillarity and gravity due to the interface deflection, respectively. A similar boundary condition but for a Newtonian liquid may be found in many papers, e.g., in Pérez-Garcia and Carneiro [36].

We note that the surface tension $\bar{\sigma}^*$ appears effectively only in the first term of the right-hand side of Eq. (8d). Since $\bar{\sigma}^*$ varies along the layer interface due to a nonuniform interfacial temperature, the above-mentioned term produces an extra component containing γ. However, since the corresponding term contains the coefficient $\gamma \Delta T^*/\sigma_0$, which is normally small for moderate values of temperature difference ΔT^*, it will be further neglected.

The most important feature of the analysis presented below which is absent in previous work is deformability of the layer interface. Its presence is quantified by surface tension and in dimensionless form by the capillary number, Ca: If the interface is nondeformable, then Ca = 0, whereas if the latter is nonzero, then the interfacial deformability becomes more pronounced with its increase. Note that surface tension $\bar{\sigma}^*$ appears also in Bond number, Bo, but the pair Bo-Ca may be replaced by G-Ca, so the capillary number will be the only representative for surface tension.

Equations (5)–(8) yield the dimensionless base state of the system,

$$\bar{\mathbf{v}} = 0, \quad \bar{T} = -z + T_0. \tag{10}$$

Next, infinitesimally small perturbations are imposed on the base-state Eq. (10) to carry out the linear stability analysis of the system. It can be proved that Squire's theorem is applicable in the present case. Thus in what follows, only two-dimensional disturbances are considered. The governing equations are then linearized around the base-state Eq. (10) and normal modes

$$f'(\mathbf{x}, t) = \tilde{f}(z) \exp(ikx + st), \quad \xi(x, t) = \tilde{\xi} \exp(ikx + st), \tag{11}$$

are substituted, where $f'(\mathbf{x}, t)$ is the perturbation to a dynamic quantity $f(\mathbf{x}, t)$, such as the components of the fluid velocity field v_x and v_y, the stress tensor $\boldsymbol{\tau}$, pressure p, and temperature T; $\tilde{f}(z)$ is the corresponding eigenfunction in the Laplace-Fourier space; and $\tilde{\xi}$ is a constant. The parameters k and $s = s_r + is_i$ are the wave number of the perturbations in the x direction and its complex growth rate, respectively. The flow is linearly unstable if at least one eigenvalue satisfies the condition $s_r > 0$.

As a result of this procedure, the linearized continuity, momentum conservation, and heat advection-conduction equations become

$$ik\tilde{v}_x + D\tilde{v}_z = 0, \tag{12a}$$

$$\frac{1}{\mathrm{Pr}} s\tilde{v}_x = -ik\tilde{p} + ik\tilde{\tau}_{xx} + D\tilde{\tau}_{xz}, \tag{12b}$$

$$\frac{1}{\mathrm{Pr}} s\tilde{v}_z = -D\tilde{p} + ik\tilde{\tau}_{xz} + D\tilde{\tau}_{zz}, \tag{12c}$$

$$s\tilde{T} - \tilde{v}_z = (D^2 - k^2)\tilde{T}, \tag{12d}$$

where $D = \frac{d}{dz}$. The stresses in Eqs. (12) satisfy the Jeffreys constitutive relation

$$(1 + L_1 s)\tilde{\tau}_{xx} = 2ik(1 + L_2 s)\tilde{v}_x, \tag{13a}$$

$$(1 + L_1 s)\tilde{\tau}_{xz} = (1 + L_2 s)(D\tilde{v}_x + ik\tilde{v}_z), \tag{13b}$$

$$(1 + L_1 s)\tilde{\tau}_{zz} = 2(1 + L_2 s)D\tilde{v}_z. \tag{13c}$$

Equations (12) and (13) are then supplemented with two sets of boundary conditions. At $z = 0$, assumption of Navier slip [38] and impermeability at the plate implies

$$\tilde{v}_x = \zeta \tilde{\tau}_{xz}; \quad \tilde{v}_z = 0; \quad \tilde{T} = 0; \tag{14a}$$

At the deformable boundary, due to the presence of the Marangoni forces additional stresses are generated. Thus, based on the standard procedure of projection of the boundary conditions at the

deformed interface $z = \xi$ onto $z = 1$, the boundary conditions at $z = 1$ read

$$\tilde{v}_z = s\tilde{\xi}, \tag{14b}$$

$$\tilde{\tau}_{xz} = -ik\mathrm{Ma}(\tilde{T} - \tilde{\xi}), \tag{14c}$$

$$-\tilde{p} + \tilde{\tau}_{zz} = -\frac{(\mathrm{Bo} + k^2)}{\mathrm{Ca}}\tilde{\xi}, \tag{14d}$$

$$D\tilde{T} + \mathrm{Bi}(\tilde{T} - \tilde{\xi}) = 0. \tag{14e}$$

Equations (12)–(14) constitute a generalized linear eigenvalue problem which is to be solved for the eigenvalues s and the eigenfunctions for a specified set of parameter values Bi, Bo, Ca, L_1, L_2, Pr, and Ma. To determine the spectrum of the eigenvalue problem (12)–(14) the pseudospectral method is employed and its details are presented in Appendix.

III. RESULTS AND DISCUSSION

In this section, we present the results of our investigation. Sections III A and III B are devoted to the case with no slippage at the substrate, whereas Sec. III C contains the results for the case with slippage.

A. Dilute polymer solutions

The previous studies [7,9–11,36] on Marangoni instability in a layer of a Newtonian fluid with a deformable surface showed the predominant emergence of the stationary mode which is characterized by $s_i = 0$, implying nontraveling disturbances at the onset of instability. Here the numerical approach employed to solve the present problem is validated by comparing with the results available in literature or with some analytical results and results obtained from the numerical computations for the stationary mode.

The neutral stability curve for the stationary mode in the case with no slippage, $\zeta = 0$, can be obtained analytically by substituting $s = 0$ into the governing equations (12)–(14) and the resulting dispersion relation in terms of the Marangoni number, Ma, in the form [9] is

$$\mathrm{Ma} = -\frac{8k(\mathrm{Bo} + k^2)[k\cosh(k) + \mathrm{Bi}\sinh(k)][k - \cosh(k)\sinh(k)]}{-k^3[\mathrm{Bo} + (1 - 8\mathrm{Ca})k^2]\cosh(k) + (\mathrm{Bo} + k^2)\sinh^3(k)}. \tag{15}$$

It can be immediately deduced from Eq. (15) that the neutral Marangoni number and its critical value (if the instability is indeed stationary) Ma_c are independent of Pr, L_1, and L_2. This feature stems from the fact that along the neutral stability curve for the stationary mode $s = 0$, and therefore the parameters Pr, L_1, and L_2 appearing in the eigenvalue problem (12)–(14) only in association with s cannot affect the neutral stability curve for a stationary mode. This implies that the critical conditions for the stationary mode for a Jeffreys fluid remain the same as in the case of a Newtonian fluid. The variation of Ma with k given by Eq. (15) is presented in Fig. 1 for a fixed set of parameters. The critical value of the Marangoni instability Ma_c is obtained by minimizing $\mathrm{Ma}(k)$ and the critical wave number k_c is determined then as $\mathrm{Ma}_c = \mathrm{Ma}(k_c)$.

For the stationary mode with $\mathrm{Bi} = 0$, $\mathrm{Bo} = 0.1$, and $\mathrm{Ca} = 0.01$, the critical Marangoni number $\mathrm{Ma}_c = 6.6667$ as obtained by Pérez- Garcia and Carneiro [36] is in agreement with the value of Ma_c obtained from Eq. (15). To validate our numerical code, the neutral stability curve determined both via Eq. (15) and numerically is presented in Fig. 1, which exhibits an excellent agreement between the two.

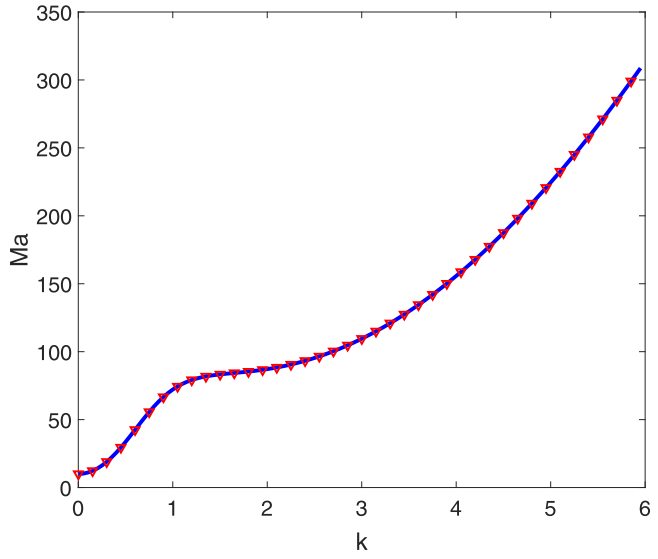

FIG. 1. Variation of Ma with k for the stationary mode in a layer of a Newtonian fluid with $\mathrm{Bi} = 0$, $\mathrm{Bo} = 0.1$, $\zeta = 0$, and $\mathrm{Ca} = 0.01$. The figure also presents a validation of our numerical approach. The continuous curve is obtained from the analytical expression (15), whereas the dots are obtained numerically. The system is unstable for Ma in the domain above the curve.

Along with the stationary modes, the present system may also exhibit oscillatory modes due to the viscoelastic nature of the fluid. Our numerical method is also validated for the oscillatory modes in Fig. 2 by assuming zero gravity $\mathrm{Bo} = 0$ and infinite surface tension $\mathrm{Ca} = 0$ which corresponds to

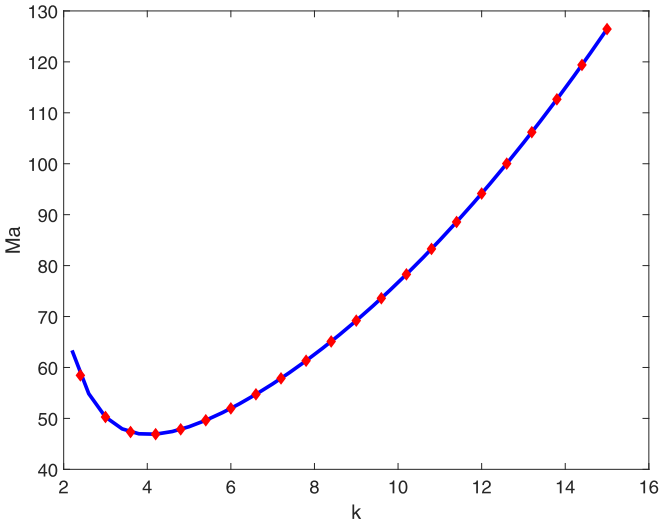

FIG. 2. The variation of Ma with the wave number k for the oscillatory mode in a layer of Jeffreys fluid with a nondeformable interface at $\mathrm{Bo} = 0$, $\mathrm{Ca} = 0$, $\mathrm{Bi} = 0$, $L_1 = 0.2$, $\zeta = 0$, and $L_2 = 0.01$. The continuous curve is obtained using our numerical method, whereas the dots represent the data extracted from the results by Lebon *et al.* [19]. The figure also presents a validation of our numerical method for the oscillatory mode exhibited by a Jeffreys fluid with a nondeformable surface.

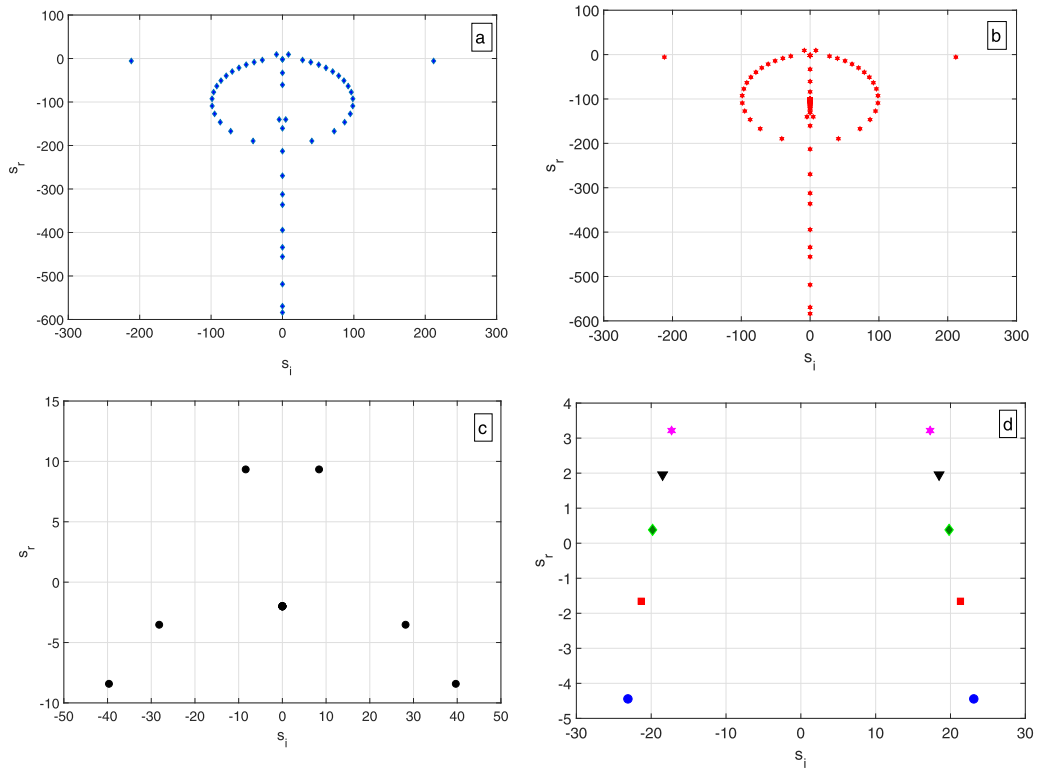

FIG. 3. [(a)–(c)] The eigenvalue spectrum of the problem Eqs. (12)–(14) for $k = 4$, Bi $= 0$, Bo $= 0.1$, $L_1 = 0.5$, $L_2 = 0.01$, Ma $= 40$, $\zeta = 0$, and Ca $= 0.01$. Panels (a) and (b) present the full spectrum of the problem obtained for $N = 50$ and $N = 75$ collocation points, respectively. (c) Close-up of panel (b) in the vicinity of $s = 0$ to emphasize the emergence of two unstable oscillatory modes with $s_r > 0$ and $s_i \neq 0$. The discrete modes at $s_i \sim 0$ are stable stationary modes independent of the viscoelasticity of the fluid. The balloon constitutes the continuous spectrum part of the problem, whereas the present discrete modes representing stationary and oscillatory modes are spread all over the spectrum. Panel (d) shows the variation of the leading eigenvalues of the problem with a variation of the dimensionless relaxation parameter L_1 for the rest of parameters as specified for panels (a)–(c). The modes from the bottom to top correspond to $L_1 = 0.15,\ 0.175,\ 0.2,\ 0.225$, and 0.25, respectively. The oscillatory modes become stable with a decrease in L_1. Note that stationary modes are not shown here to focus on the oscillatory modes since the effect of L_1 on the stationary mode is negligible.

a nondeformable free surface of the layer. Here the results obtained for the Marangoni instability in a Jeffreys fluid by Lebon *et al.* [19] are compared with those obtained by our numerical method. The perfect agreement between the results validates our numerics in the case of the oscillatory modes as well.

Before further presenting the results on the onset of the Marangoni instability it is essential to analyze the eigenvalue spectrum of the problem. Figures 3(a) and 3(b) show the full spectrum and its close-up around the value of $s = 0$, i.e., $s_r = s_i = 0$, to emphasize the emergence of unstable oscillatory modes. The full spectrum of the problem may be subdivided into the *continuous* and *discrete* parts. The continuous spectrum arises due to the singularity present in the Jeffreys constitutive relation [39]. After substitution of the normal modes, the singularity emerges in the coefficient $1 + L_1 s$ multiplying the stresses. Thus, the continuous spectrum is defined by the relation, $s = -1/L_1$. Mathematically, the continuous spectrum is expected to be a line. However, due to truncation of the Chebyshev polynomial series in the pseudospectral method, the line assumes

a ballon shape [40] shown in Figs. 3(a) and 3(b). If an eigenvalue changes significantly and/or new eigenvalues emerge with a variation in the number of collocation points, N, then it belongs to the continuous part of the spectrum. However, in the case of an eigenvalue from the discrete part of the spectrum, it exhibits small variations with respect to the change in the number of collocation points provided that the latter is sufficiently large to warrant the convergence of the results.

The unstable discrete eigenvalues of the present problem are shown in Fig. 3(c). These conjugate oscillatory modes have the same growth rate s_r; however, the frequencies s_i are of an equal absolute value but have opposite signs. Thus, one oscillatory mode induces wave propagation in the positive x direction, whereas the other one does the same but in the negative x direction. Since both oscillatory modes grow at the same rate, both are related to the same critical parameter values. Therefore, it suffices to analyze either one of the oscillatory modes to determine the critical parameters, which is indeed the case in the following results. Note that along with the unstable symmetric modes, there exist other discrete stable modes such as the pair with $s_i \sim \pm 211$ observed in Figs. 3(a) and 3(b). Such modes can be a part of the spectrum of the governing equations and boundary conditions corresponding to stable disturbances of arbitrary traveling speed and decay rate s_r. They may coexist with other stable or unstable modes. These modes are innocuous due to their stable nature and hence do not need to be studied in detail. For a Newtonian fluid, only stationary modes normally exist; however, in a viscoelastic fluid with nonzero values of L_1, oscillatory modes emerge in addition to the stationary modes. Thus, the elastic nature of the fluid gives rise to the emergence of oscillatory modes. Furthermore, Fig. 3(d) illustrates that the oscillatory modes can be destabilized by making a fluid increasingly elastic. This result indicates that the oscillatory instability found in the present work could be a result of the coupling between the elastic stresses introduced by the relaxation term in the constitutive equation and Marangoni stresses caused by the temperature dependence of the surface tension of the fluid. It is important to note here that the mere emergence of oscillatory instability with an increase in the relaxation time of a viscoelastic fluid instead of stationary instability was also found by Getachew and Rosenblat [18] but for a layer with a nondeformable interface. Therefore, the emergence of the oscillatory instability is not related to the interface deformability but to viscoelasticity. The fact that the stationary mode may become long wave instead of a finite-wavelength [18] is due to deformability.

The contour plots of v_x' and v_z' and temperature T' corresponding to the leading eigenvalue for the oscillatory instability are shown in Fig. 4. These eigenfunctions have been normalized by their respective maximal absolute values. The velocity eigenfunctions are essentially nonzero near and at the layer interface as a consequence of the Marangoni effect driving the instability at the layer interface. The contour lines in both the velocity and temperature disturbance fields display maximum achieved by the perturbations in the vicinity of the layer interface with respect to the domain away from it, which demonstrates the source of the instability lying at the interface. Figure 4(c) shows the perturbed temperature field that substantially deviates from zero toward the layer interface. We note in passing that the perturbed temperature field can be well approximated by a cubic polynomial in z in contrast to the base-state temperature, which is a linear function of z.

As shown in Sec. III D, the energy analysis of the perturbations reveals a major role of both the Marangoni stresses acting at the free surface and bulk stresses in introducing the oscillatory instability. The maximal value of each field attained by the perturbation amplitude near the interface shown in Fig. 4 is clearly due to the presence of the Marangoni stresses. Thus, the contour plots emphasize in this case the role of the Marangoni stresses in causing the oscillatory instability, although, they do not glean much information about the role of the bulk stresses in the emergence of the oscillatory instability. The Marangoni stresses also play a big role in destabilizing the stationary mode as revealed in the energy analysis of Sec. III D.

In the present work, the Marangoni instability emerging in the polymer solutions dissolved in a water solvent is analyzed. In this case, the typical ranges for the physical properties are [6,25,41] $d \sim 10^{-6}$–10^{-3} m, $\rho \sim 10^3$ kg/m^3, $\bar{\sigma}^* \sim 10^{-3}$–$10^{-1}$ N/m, $\gamma \sim 10^{-5}$–10^{-3} N/(m K), $k_{\text{th}} \sim 10^{-6}$–$10^{-3}$ J/(m s K), $q \sim 1$–10^2 J/(m^2 s K), $\alpha \sim 10^{-7}$–10^{-5} m^2/s, $\mu \sim 10^{-3}$–10^2 Pa s,

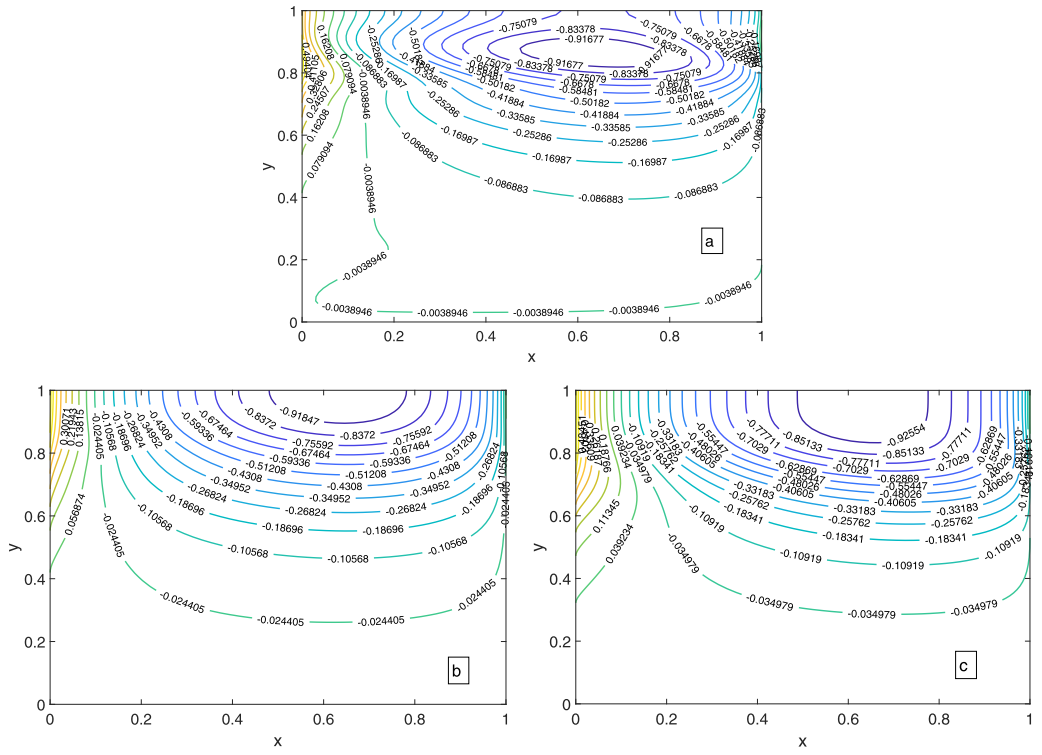

FIG. 4. Normalized contour plots for the oscillatory instability mode with $\mathrm{Bi} = 0$, $\mathrm{Bo} = 0.1$, $L_1 = 0.5$, $L_2 = 0.01$, $\mathrm{Ma} = 40$, $\zeta = 0$, $k = 4$, and $\mathrm{Pr} = 7$. The x domain of $0 \leqslant x \leqslant 2\pi/k$ is normalized to the interval [0,1], which is also the interval of the z axis. Panels (a)–(c) represent the contour plots of the perturbed velocities v_x' and v_z' and the temperature T', respectively. Here $v_x' = \mathrm{Re}[\tilde{v}_x \exp(ikx)]$, $v_z' = \mathrm{Re}[\tilde{v}_z \exp(ikx)]$, and $T' = \mathrm{Re}[\tilde{T} \exp(ikx)]$. Essentially nonzero values of the perturbation velocities, v_x' and v_z', concentrate near and at the layer interface $z = 1$ and serve as an evidence that the flow is driven by the Marangoni stresses there.

$\lambda_1 \sim 10^{-7}$–10^{-1} s, and $\lambda_2 \sim 10^{-7}$–10^{-3} s. In the case of dilute solutions, the typical dimensionless numbers are $\mathrm{Bi} \sim O(10^{-3} - 10)$, $\mathrm{Bo} \sim O(0.001 - 0.1)$, $\mathrm{Ca} \sim O(0.0001 - 0.1)$, $L_1 \sim O(0.01 - 1)$, $L_2 \sim O(0.001 - 0.01)$, and $\mathrm{Pr} \sim O(1 - 10)$. This parametric range will be used here to study the various modes of instability.

Before proceeding with the stability analysis of the oscillatory modes, the effect of the variation of the capillary number Ca on the stationary modes needs to be studied to facilitate the subsequent discussion. For a further discussion, the characterization of the stationary instability mode is subdivided into two segments, viz., a low-wave-number or long-wave (LW) instability confined to $k \ll 1$ and a finite-wave-number or short-wave (SW) instability constrained to $k \sim 1$ to identify the effect of variation in the different ranges of the dimensionless numbers k on the stationary mode. The neutral stability curves for a fixed parameter set with a varying Ca for the stationary mode in a layer of a Newtonian liquid are shown in Fig. 5. As readily seen, an increase in Ca has a strong effect on the LW mode. For $\mathrm{Ca} < 0.0087$, SW instability dominates the stability behavior with critical values $k_c \sim 2$ and $\mathrm{Ma}_c \sim 79.6$. This range is close to the conducting mode of a layer with the nondeformable interface considered by Pearson [7]. However, for $\mathrm{Ca} > 0.0087$, the deformational mode becomes dominant and the LW instability determines the system stability with $k_c = 0$. Since $k_c = 0$ for the LW instability, thus, it follows from Eq. (15),

$$\mathrm{Ma}_c = \frac{2}{3}\frac{(1 + \mathrm{Bi})\mathrm{Bo}}{\mathrm{Ca}}. \tag{16}$$

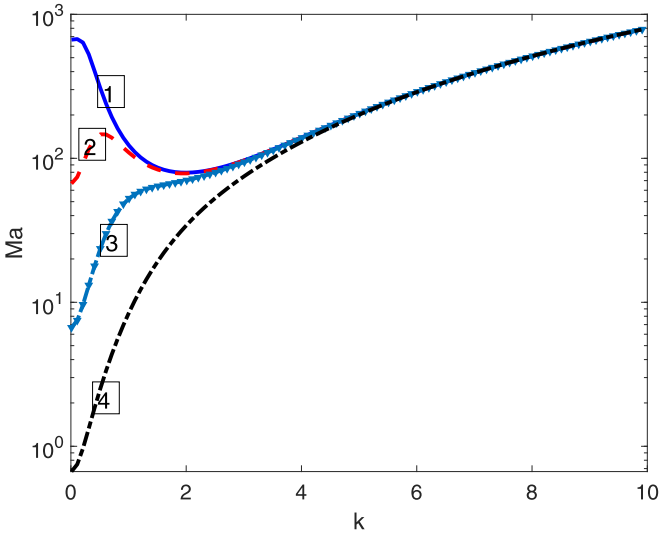

FIG. 5. Neutral stability curves showing variation of Ma with the disturbance wave number k for the stationary mode with $\mathrm{Bi} = 0$, $\mathrm{Bo} = 0.1$, $L_1 = 0$, $L_2 = 0$, $\zeta = 0$, and $\mathrm{Pr} = 7$. Curves 1 to 4 correspond to $\mathrm{Ca} = 0.0001$, 0.001, 0.01, and 0.1, respectively. An increase in Ca, i.e., in surface deformability has a strong effect on the LW part of the neutral stability curve transforming the finite-wavelength instability to the long-wave one. The domain of instability is located above the curves.

It is quite clear from Eq. (16) that the transition of the dominant mode from the stationary SW or from oscillatory instability (if exists, see below) depends strongly on both Bo and Ca and weakly on Bi, since the latter is usually small. This transition of the dominant mode also helps in determining the parameter regime for the applicability of the long-wave analysis [1].

The neutral stability curves for the oscillatory modes are shown in Fig. 6. The destabilization of the system taking place with an increase in Ca is understood via an associated weakening in the

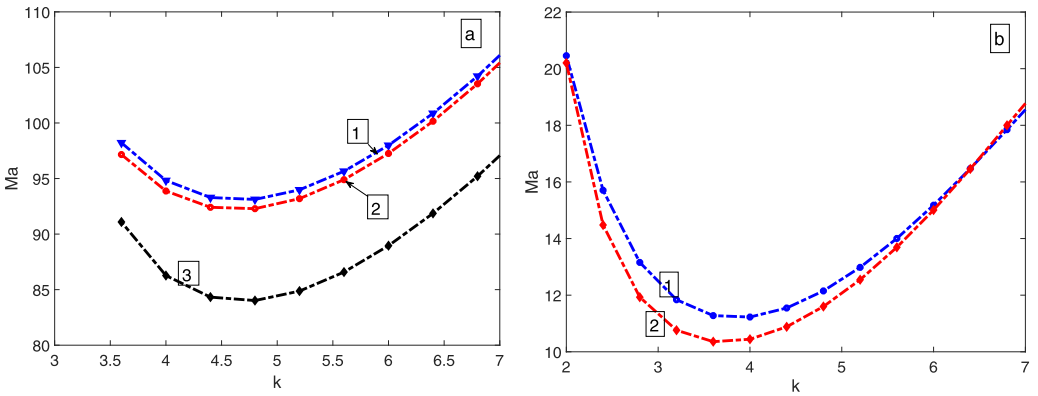

FIG. 6. Neutral stability curves displaying the variation of Ma with the wave number k for the oscillatory mode at $\mathrm{Bi} = 0$, $\mathrm{Bo} = 0.1$, $L_2 = 0.01$, $\zeta = 0$, and $\mathrm{Pr} = 7$. (a) For $L_1 = 0.1$, curves 1–3 correspond to $\mathrm{Ca} = 0.001$, 0.01, and 0.1, respectively. (b) For $L_1 = 0.5$, curves 1 and 2 correspond to $\mathrm{Ca} = 0.0001$ and 0.1, respectively. An increase in surface deformability leads to destabilization via a decrease in Ma_c for the oscillatory mode. The system is destabilized by an increase in the relaxation parameter L_1. The domain of instability is located above the curves.

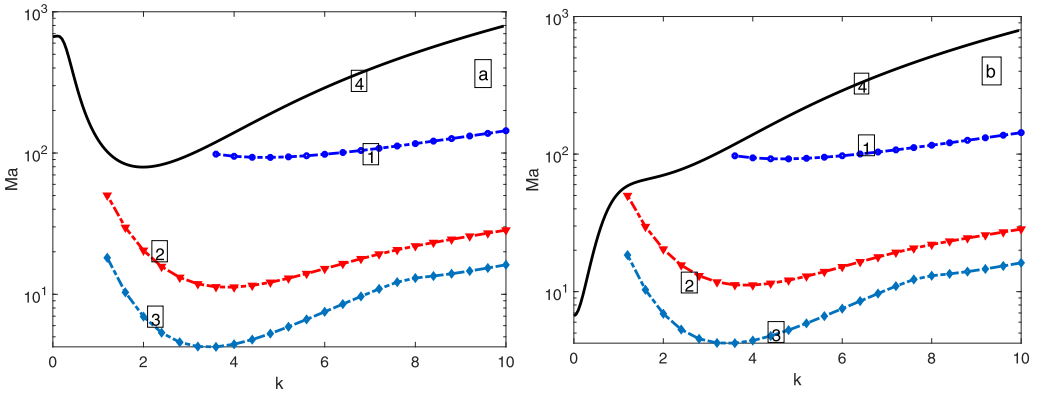

FIG. 7. The neutral stability curves in (a) for Ca = 0.0001 and (b) for Ca = 0.01 presenting variation of Ma with k for the oscillatory mode at Bi = 0, Bo = 0.1, $L_2 = 0.01$, $\zeta = 0$, and Pr = 7. Curves 1–3 in both panels correspond to $L_1 = 0.1,\ 0.5$, and 1, respectively. Curve 4 in both panels represents the neutral stability curve for the stationary mode. The figure shows that the effect of variation of the interface deformability is strong on the LW instability, whereas the effect on the oscillatory instability is relatively weaker. An increase in L_1 leads to a significant decrease in Ma_c for the oscillatory mode. The domain of instability is located above the curves in both panels.

surface tension at the free surface and its resulting enhanced deformability. Furthermore, with an increase in deformability, i.e., Ca, the minimum in the neutral stability curve corresponding to the SW instability disappears giving rise to the presence of only stationary LW instability at sufficiently high Ca, as shown in Fig. 5. A comparison between the two panels of Fig. 6 makes clear that an increase in the relaxation parameter L_1 with a fixed retardation parameter L_2 results in a significant decrease in the critical values of the Marangoni number Ma_c and the wave number k_c, and the ensuing destabilization of the system.

Neutral stability curves for a fixed Ca and a varying L_1 are presented for the oscillatory mode in Fig. 7. They exhibit a strong decrease in Ma_c associated with an increase in L_1. As noted above, the neutral stability curve for the stationary mode remains unaffected with the variation in Pr, L_1, and L_2. Thus, there is only one curve in Fig. 7 which depicts the corresponding stationary mode. It follows from Figs. 5 and 6 that an increase in Ca leads to a decrease in Ma_c for both stationary and oscillatory modes. However, Fig. 7 shows the existence of a stronger effect on the stationary mode as compared to that on the oscillatory modes, thereby making the stationary mode a dominant instability mode as Ca increases. As displayed in Fig. 7(a), for a low value of Ca, the stationary finite-wavelength mode is dominant for lower values of L_1. With an increase in L_1, the oscillatory finite-wavelength mode becomes dominant. However, as shown in Fig. 7(b) for a larger value of Ca, the long-wave stationary mode determines the onset of instability for a range of L_1 much wider than in Fig. 7(a). This long-wave mode of instability is replaced by a finite-wavelength oscillatory mode when L_1 exceeds a certain value. This aspect becomes much clearer in the following discussion where both types of modes are compared for their critical parameter values in the Ma_c-Ca plane.

A relative location of the stationary and oscillatory neutral curves determines the type of the instability onset in the system. Figure 8 presents a summary of the variation of the critical values of the Marangoni number Ma_c and the wave number k_c with the capillary number Ca. Figure 8(a) shows the stationary mode either SW or LW as the dominant mode of instability for $L_1 < 0.1$, whereas for $L_1 > 0.1$ the scenario is more complex. In this range, there exists an upper limit on Ca, $\mathrm{Ca} = \mathrm{Ca}_u$ below which for $\mathrm{Ca} < \mathrm{Ca}_u$ the oscillatory mode sets in first in the system. Above this value, for $\mathrm{Ca} > \mathrm{Ca}_u$ the instability is LW. Also, the value of $\mathrm{Ca} = \mathrm{Ca}_u$ above which the LW mode dominates the instability of the system increases with an increase in L_1. On the physical grounds, this property implies that if the fluid is sufficiently elastic, i.e., polymer concentration in the solution

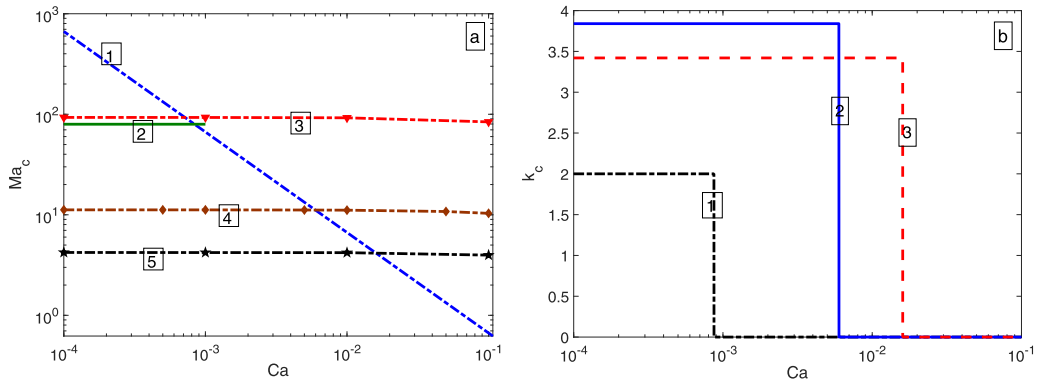

FIG. 8. Variation of the critical parameters with Ca at Bi = 0, Bo = 0.1, $L_2 = 0.01$, $\zeta = 0$, and Pr = 7. Panels (a) and (b), respectively, display the variation of the critical values Ma_c and k_c of the dominant mode with Ca. (a) Curves 1 and 2 show the critical Marangoni number for the stationary instability, long wave and short wave, respectively. Curves 3–5 correspond to the oscillatory instability for $L_1 = 0.1,\ 0.5$, and 1, respectively. Note that the points of intersection between the diagonal LW curve and the horizontal lines for either stationary SW or oscillatory modes represent codimension-two points of the system. (b) Curve 1 corresponds to the stationary instability, curves 2 and 3 correspond to the oscillatory instability for $L_1 = 0.5$ and 1, respectively. The steplike drop in the curves is due to the switching of the dominant mode from the SW or oscillatory instability to the LW stationary instability. The figure illustrates the effect of surface deformability on the parameter domains where SW, LW, and oscillatory instabilities are dominant.

is sufficiently high, then the oscillatory mode is likely to be observed before the stationary mode, as long as an increase in the capillary number is concerned. In the case of a nondeformable surface Ca = 0, thus, with $L_1 > 0.1$ the oscillatory mode of the instability dominates without a competition from LW. However, interface deformability affects the parametric regimes in which the oscillatory mode is dominant. Hence, interface deformability is crucial for selection of the dominant instability mode. Note that the points of intersection between the diagonal LW curve and the horizontal lines for either stationary SW or oscillatory modes represent codimension-two points of the system. The corresponding variation of the critical wave number k_c with Ca is depicted in Fig. 8(b), where sudden jumps from a finite k_c value to $k_c = 0$ illustrates the transition of the instability mode from the SW instability or an oscillatory mode to the stationary LW instability. In the range of $L_1 < 0.1$, since the stationary mode dominates the system instability, the corresponding curves depicting k_c variation with Ca coincide with curve 1 in Fig. 8(b).

To this point, we have presented the results obtained for an effectively insulated free surface, i.e., for a vanishing Biot number, Bi. However, depending on the relative values of h, d, and k_{th}, the system has a finite Biot number. To illustrate the effect of variation in the Biot number, Fig. 9 presents neutral stability curves for both stationary and oscillatory modes for three values of Bi. It follows from Eq. (16) that the Biot number affects the LW instability through the term 1 + Bi. Thus, for the Biot number to impart a significant effect on the LW instability, it has to have an order unity value. This is the reason that the effect of the Biot number variation is marginal, as seen in Fig. 9(a). In the case of the oscillatory mode, similarly to the stationary mode, the effect of an increase in the Biot number is stabilizing. An enhancement in the heat transfer at the free surface and an ensuing increase in the Biot number Bi could explain the stabilizing effect observed in Fig. 9(b),

From the discussion above, it is immediately clear that the stability picture shown in Fig. 8 will be slightly altered with a small change in the Biot number, for example, for Bi = 0.5. This is indeed the reason that the effect of the Biot number as seen in Fig. 10 is marginal. The major difference between Figs. 8(a) and 10 is the presence of the overlap of the curves for the SW stationary and oscillatory modes for $L_1 = 0.1$ in the latter which represents the emergence of a codimension-three

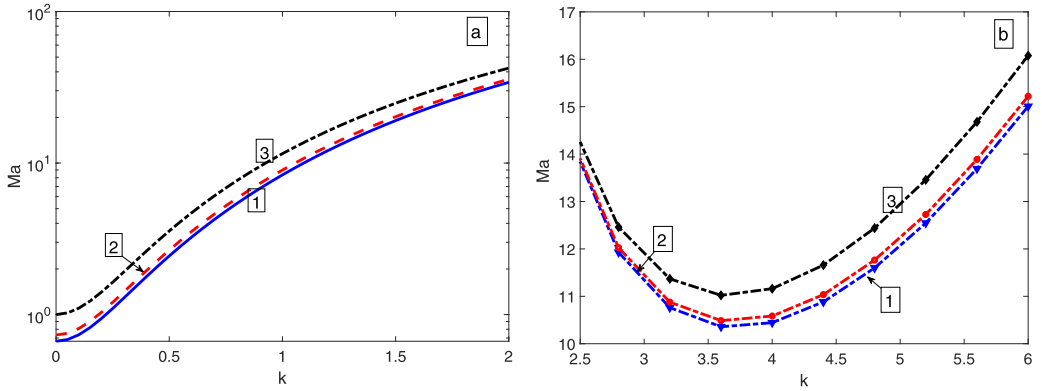

FIG. 9. Neutral stability curves for stationary (a) and oscillatory (b) modes at Ca = 0.1, Bo = 0.1, L_1 = 0.5, $L_2 = 0.01$, $\zeta = 0$, and Pr = 7. An increase in Bi leads to an increase in Ma_c for both stationary and oscillatory modes. Curves 1–3 in both panels correspond to Bi = 0, 0.1, and 0.5, respectively. The domain of instability is located above the curves in both panels.

point. This overlap phenomena occurs because of the relatively lesser stabilization of the oscillatory modes as compared to the SW instability with an increase in Bi.

Similarly to the variation in Bi, next the effect of the variation in the Bond number, Bo, on the instability is investigated. The Bond number, Bo, representing the ratio of gravitational forces to the capillary forces, can be as low as 0.001 depending on the solvent fluid and a polymer used to prepare a viscoelastic liquid. The effect of the variation in Bo on the neutral stability curves for both stationary and oscillatory modes is shown in Fig. 11. A decrease in Bo has a strong effect on the

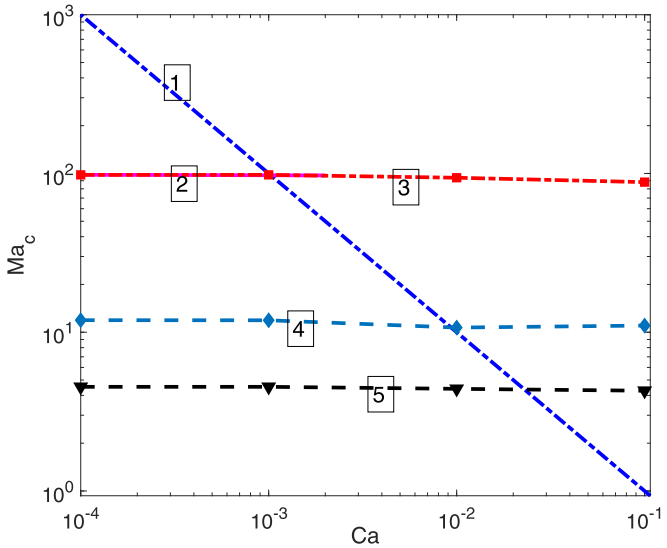

FIG. 10. Variation of Ma_c with Ca for both stationary and oscillatory modes for Bi = 0.5, Bo = 0.1, L_2 = 0.01, $\zeta = 0$, and Pr = 7. An increase in Ma_c due to an increase in Bi is clearly observed in comparison with Fig. 8 where Bi = 0. Curves 1 and 2 correspond to the long-wave and finite-wavelength stationary instability, respectively. Curves 3–5 correspond to the oscillatory instability for $L_1 = 0.1$, 0.5, and 1, respectively. The major difference between Figs. 8(a) and 10 is the presence of the overlap of the curves for the SW stationary and oscillatory modes for $L_1 = 0.1$ in the latter which represents the emergence of a codimension-three point.

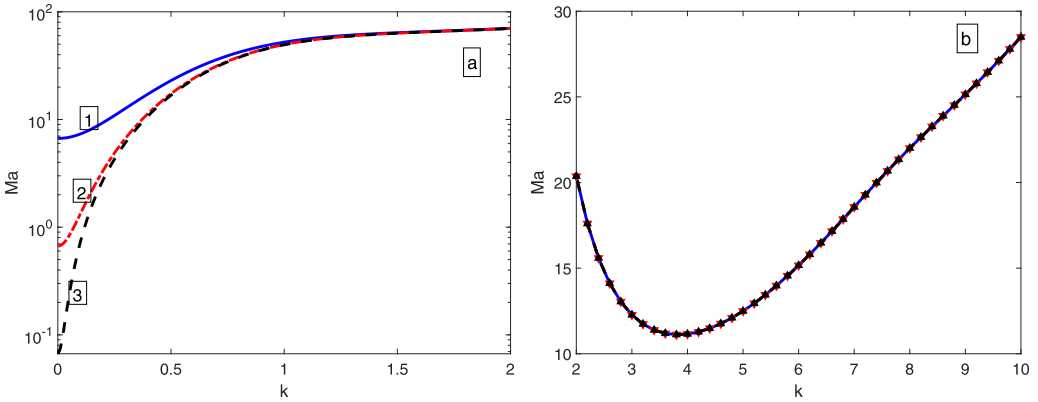

FIG. 11. Neutral stability curves for (a) stationary and (b) oscillatory modes for Ca = 0.01, Bi = 0, $L_1 = 0.5$, $L_2 = 0.01$, $\zeta = 0$, and Pr = 7. An increase in Bo has a strong effect on the LW instability. The impact on the SW instability is negligibly small effect. (a) Curves 1 to 3 correspond to Bo = 0.001, 0.01, and 0.1, respectively; (b) the three curves corresponding to Bi = 0.001, 0.01, and 0.1 overlap. This implies a negligible effect of variation in Bo on the oscillatory mode. Panel (a) illustrates the effect of variation in interface deformability as a consequence of variation in interfacial stress relative to the gravitational one on the stationary mode. The instability domain is located above the curves in both panels.

LW part of the stationary mode but as k increases, the effect of variation in Bo becomes negligible as shown in Fig. 11(a). The threshold value of the Marangoni number decreases with an increase in Bo.

For the oscillatory modes, similarly to the stationary SW modes, a variation in Bo has a negligible effect on the neutral stability curves. A decrease in Bo is equivalent to an increase in surface tension compared to the gravity effect, corresponding therefore to a more deformable interface. But the relative deformability introduced by the decreasing Bond number affects selectively the LW instability, while producing a negligible effect on the stationary SW and oscillatory modes which can be explained as follows. In the case of the LW disturbance $k \to 0$, the impact of gravity is much stronger than that of surface tension. In the same vein, Bo appears only as $\mathrm{Bo} + k^2$ in the normal-stress boundary condition at the deformable surface, Eq. (14d), and Bo explicitly appears in the expression for Ma_c for the LW instability, Eq. (16). However, for $k \gg \mathrm{Bo}$, the effect of Bo becomes negligible, thereby exhibiting the behavior shown in Fig. 11. In summary, in the presented range of Bond numbers, the instability is long wave.

B. Concentrated polymer solutions

The results presented in Sec. III A have been obtained for dilute aqueous polymer solutions. In polymer processing industries, highly concentrated polymer solutions or polymer melts are frequently encountered. These viscoelastic fluids are characterized by higher viscosities and the relaxation time constants, as compared to those of the dilute solutions. Due to an increase in the rheological properties these fluids possess high values for Pr and L_1, of order 1000 and 10, respectively. Additionally, an increase in the polymer concentration also implies a decrease in L_2 down to 0.0001 for polymer melts. This subsection deals with concentrated polymer solutions.

Figure 12 displays the neutral stability curves for the typical values of L_1 and L_2 of concentrated polymers solutions. Note that a change in Pr from 7 to 200 does not have any significant effect on the qualitative features of the stationary and oscillatory modes. For higher polymer concentrations the values of $L_1 = 10$ and $L_2 = 0.001$ are possible and this fact leads to a drastic decrease in Ma_c for the oscillatory mode. As a consequence of this, oscillatory modes can become dominant even for Ca > 0.01 unlike in dilute solutions.

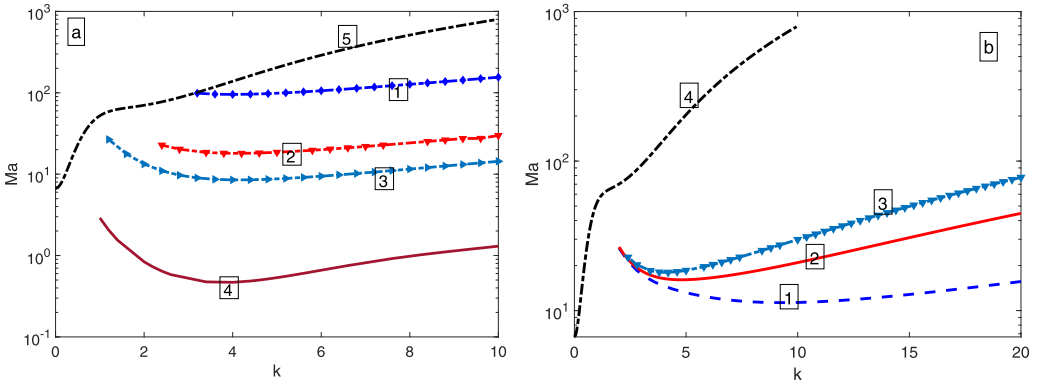

FIG. 12. Neutral stability curves for Ca $= 0.01$, Bi $= 0$, $\zeta = 0$, and Pr $= 200$. (a) $L_2 = 0.01$ with varying L_1. Curves 1–4 correspond to $L_1 = 0.1,\ 0.5,\ 1$, and 10, respectively, whereas curve 5 is for the stationary instability. (b) $L_1 = 0.5$ with varying L_2. Curves 1–3 correspond to $L_2 = 0.001,\ 0.005$, and 0.01, respectively, whereas curve 4 is for the stationary instability. These results differ from those obtained for dilute aqueous solutions due to the presence of higher values of L_1 and lower values of L_2. Both panels show a decrease in Ma_c with either an increase in L_1 or a decrease in L_2. The domain of instability is located above the curves in both panels.

To further explore the effect of variation in Pr on the oscillatory mode of instability, the variation of Ma_c with respect to Pr is presented in Fig. 13. As shown, with Pr > 5 both the critical values of the Marangoni number, Ma_c, and the wave number k_c are approximately constant. Thus, the conclusions drawn for the dilute aqueous polymer solutions (Pr $= 7$) regarding the effect of variation in the parameter values are applicable even for the concentrated polymer solutions.

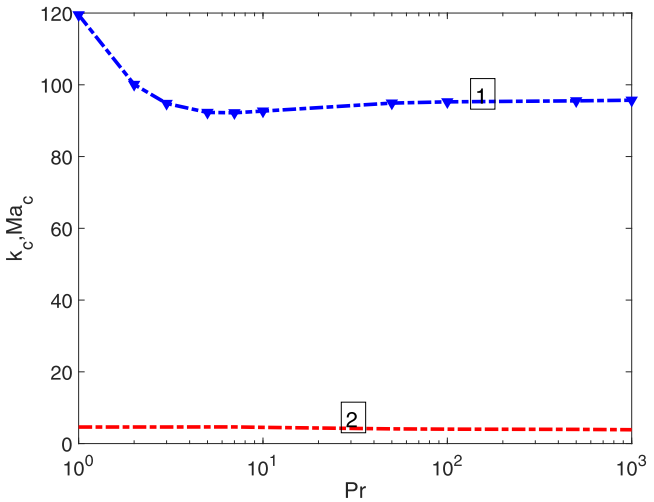

FIG. 13. Variation of the critical values for the disturbance wave number k_c and the Marangoni number, Ma_c, with the Prandtl number, Pr, for oscillatory modes with Bi $= 0$, Bo $= 0.1$, Ca $= 0.01$, $\zeta = 0$, $L_1 = 0.1$, and $L_2 = 0.01$. Curves 1 and 2 correspond to Ma_c and k_c, respectively. For Pr > 5, the dependence of Ma_c and k_c with Pr is weak. Thus, the conclusions drawn for dilute solutions are applicable also for concentrated polymer solutions with quantitative changes.

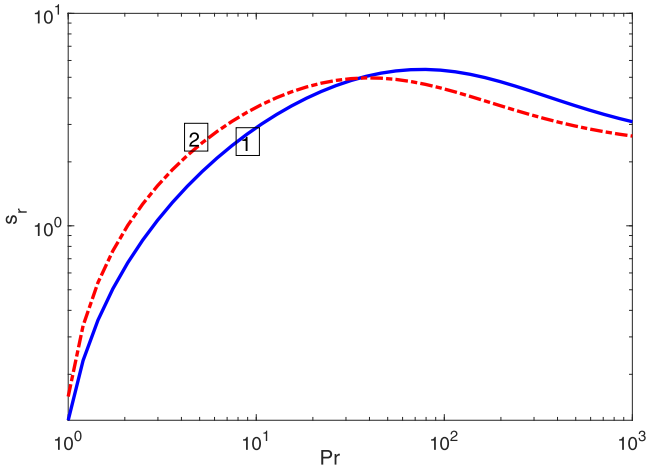

FIG. 14. Variation of the growth rate, s_r, with Pr for oscillatory modes at Bi = 0, Bo = 0.1, Ca = 0.001, and $L_2 = 0.01$. Curves 1 and 2 are for $L_1 = 1$, Ma = 10, and $L_1 = 0.5$, Ma = 20, respectively. The growth rate s_r is nonmonotonic with the variation of Pr for an oscillatory mode. Thus, although Pr does not have a strong effect on the critical parameters, it strongly affects the growth rate.

Besides a negligible effect on the critical parameters, variation in Pr has no effect on the growth rate for the stationary mode similar to a Newtonian fluid. However, variation in Pr strongly affects the growth rate, s_r, of the oscillatory modes as shown in Fig. 14. The nonmonotonic variation of the growth rate with Pr depicted in Fig. 14 shows that although Pr does not have a strong effect on the critical parameters for the oscillatory modes, it strongly affects their growth rate. Thus, concentrated polymer solutions exhibit oscillatory modes with higher growth rates compared to dilute polymer solutions since the former display higher values of Pr due to their higher viscosity. To conclude, the Marangoni instability in concentrated polymer solutions differ from that in dilute polymer solutions because of higher values of Pr and L_1 and lower values for L_2 which not only affect the critical parameters but also the growth rate of the disturbances. The effect of these parameters is presented in Fig. 12, thereby completing the thermocapillary stability analysis for both dilute and concentrated polymer solutions.

C. Effect of slippage at the substrate

In this subsection, we study the effect of slippage at the substrate expressed in terms of the dimensionless parameter ζ on the stationary and oscillatory modes of instability. It must be noted that for the processes such as additive manufacturing, various fluid-flow models require slip parameter ζ as high as 10 [42]. In other cases, such as flows past hydrophobic and grooved surfaces, ζ ranges from 0.001 to 0.1 [38]. The effect of the basal slip on the critical parameters in the case of the stationary mode is shown in Fig. 15(a): It is stabilizing for higher values of Ca, e.g., Ca = 0.01, and destabilizing for lower ones, e.g., Ca = 0.0001. In the case of Ca = 0.01, the instability is long wave and variation in ζ affects only the critical Marangoni number Ma_c, whereas the critical wave number $k_c = 0$ for the LW mode remains unaffected in the entire range of the slip coefficient ζ. Thus, the long-wave nature of the stationary instability remains unaffected by the presence of slippage at the substrate and variation of the slip coefficient ζ. As observed in Fig. 15(a) an increase in the value of the slip coefficient ζ leads to an increase in Ma_c for the LW stationary mode, whereas in the case of the finite-wave stationary mode with Ca = 0.01, an increase of slippage causes a decrease in both Ma_c and k_c.

In the case of oscillatory instability, an increase in ζ has a nonmonotonic effect on the critical parameters as shown in Fig. 15. Initially, for lower values of ζ, its increase leads to a moderate

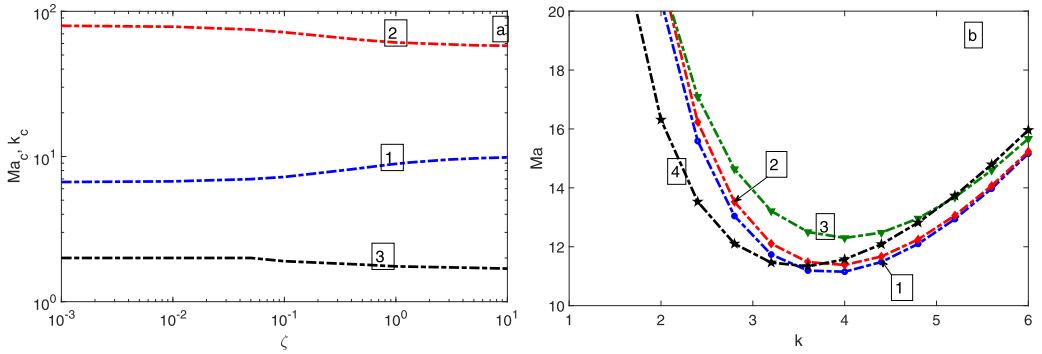

FIG. 15. (a) Variation of the critical Marangoni number, Ma_c, and the critical wave number k_c with the slip parameter ζ in the case of the stationary mode. Curves 1 and 2 correspond to $\mathrm{Ma}_c(\zeta)$ for $\mathrm{Ca} = 0.01$ and $\mathrm{Ca} = 0.0001$, respectively. Curve 3 depicts variation of k_c for the shortwave instability with $\mathrm{Ca} = 0.0001$. Note that instability for $\mathrm{Ca} = 0.01$ is long wave for the entire range of ζ. (b) Neutral stability curves in the case of the oscillatory mode for $\mathrm{Ca} = 0.01$, $L_1 = 0.5$, and $L_2 = 0.01$. Curves 1–4 correspond to $\zeta = 0$, 0.1, 1, and 10, respectively. The domain of instability is located above the curves. The other parameters for both the panels are $\mathrm{Bo} = 0.1$, $\mathrm{Bi} = 0$, and $\mathrm{Pr} = 7$.

increase in the critical values Ma_c and k_c. For $\zeta > 1$, however, a further increase in ζ at the substrate leads to a decrease in both Ma_c and k_c.

D. Mechanism for the emergence of oscillatory instability

This section explains the mechanism for the emergence of oscillatory instability found above for the case of no-slip at the substrate, i.e., $\zeta = 0$. Here we follow the approach used by Hu *et al.* [43,44].

Taking the scalar product of the linearized around $\mathbf{v} = \mathbf{0}$ version of Eq. (6) by the perturbation velocity vector $\mathbf{v}'$, integrating the result over the flow domain, and simplifying the resulting integrals yields an equation describing the time evolution of the total kinetic energy,

$$E = \int \mathbf{v}' \cdot \mathbf{v}' \, dV \tag{17}$$

in the form

$$\frac{1}{\mathrm{Pr}} \frac{\partial E}{\partial t} = -\int p' \mathbf{v}' \cdot \mathbf{n} \, dA - \frac{1}{2} \int \boldsymbol{\tau}' : \dot{\boldsymbol{\gamma}}' \, dV + \int \boldsymbol{\tau}' \cdot \mathbf{v}' \cdot \mathbf{n} \, dA \equiv -I_p - I_b + I_M, \tag{18}$$

where I_p, I_b, and I_M are the pressure work, the bulk stress work, and surface stress work (Marangoni work) components in the balance, respectively; dV and dA are the volume and area elements, respectively; and the area integrals are over the flow domain boundary. The expression $\dot{\boldsymbol{\gamma}}' = \nabla \mathbf{v}' + \nabla \mathbf{v}'^T$ represents the strain-rate tensor. Since only at the free deformable surface the velocity perturbations $\mathbf{v}'$ do not vanish, the contribution to the area integrals will come from the free surface alone. It must be noted that for a nondeformable surface the pressure integral I_p vanishes [43]. However, due to interfacial deformability, it does not vanish, and as shown below it contributes to the growth of the perturbations. The Marangoni stress work component of Eq. (18) I_M is found to be positive for the parameter values explored here, and thus it exerts a destabilizing effect. Incidentally, the bulk stress work component I_b is unconditionally positive in the case of a Newtonian fluid, since $\boldsymbol{\tau}' : \dot{\boldsymbol{\gamma}}' = 2\mu \Sigma_{i,j} \gamma_{ij}^2 \geqslant 0$, and thus results in a decrease in the perturbation energy due to the presence of viscous dissipation. Note that stationary modes may still emerge even if the bulk stress work is positive as in the case of a Newtonian fluid. These stationary modes may become unstable by virtue of the Marangoni stress work.

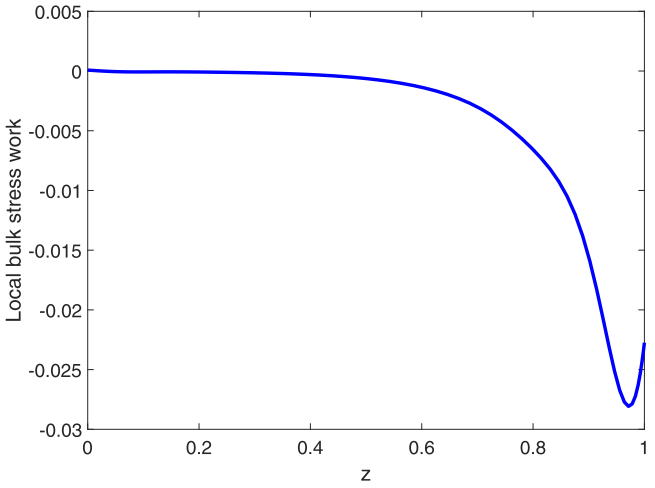

FIG. 16. Variation of the integrand of the bulk stress work component I_b of the energy balance in the layer with z for $\mathrm{Bi} = 0,\ \mathrm{Bo} = 0.1,\ \mathrm{Ca} = 0.01,\ L_1 = 0.5,\ k = 4,\ \mathrm{Ma} = 15,\ \zeta = 0,\ \mathrm{Ra} = 0$, and $L_2 = 0.01$ for the most unstable oscillatory mode. The local bulk stress work component is negative in the enture domain, and thus it causes an increase in the energy of the disturbances. Additionally, in this case the Marangoni stress work is positive and the pressure work is negative. Thus, all the three components of Eq. (18) induce the growth of the perturbation energy E.

The integrand in the bulk stress work component I_b determined numerically for the unstable oscillatory mode turns out to be negative definite, when viscoelasticity exists ($L_1,\ L_2 \neq 0$) within the liquid layer, as a function of z, as displayed in Fig. 16, which implies $I_b < 0$. Thus, to destabilize an oscillatory mode along with the Marangoni and pressure work components, the bulk stress work component caused by the elastic stresses in the fluid are essential. The values of the various components of Eq. (18) determined numerically and normalized with the Marangoni stress work I_M for the three different types of unstable modes, viz., long wave, short wave, both stationary, and two oscillatory modes, are presented in Table I. Finally, I_b is found to be of a larger magnitude than I_M and I_p in the case of unstable oscillatory modes, suggesting that the elastic forces supply via the bulk stress work a significant part of the energy required for the destabilization of the system through the oscillatory modes.

TABLE I. Sample values of the pressure work I_p and bulk stress work I_b normalized by the value of the surface stress work (Marangoni stress work) I_M for $\mathrm{Bi} = 0, \mathrm{Bo} = 0.1, \zeta = 0$, and $\mathrm{Pr} = 7$ in the case of unstable stationary long wave (the first row), stationary short wave (the second row), and oscillatory (the last two rows) modes. The component I_b switches from positive to negative as viscoelasticity of the fluid is introduced, i.e., L_1 becomes nonzero, thereby emphasizing the effect of the liquid viscoelasticity on the bulk stress work. The pressure integral I_p possesses a nonzero value as a consequence of the interface deformability.

Parameters	I_p	I_b
$L_1 = 0,\ L_2 = 0,\ k = 0.01,\ \mathrm{Ma} = 10,\ \mathrm{Ca} = 0.01$	−0.21976	0.15748
$L_1 = 0,\ L_2 = 0,\ k = 2, \mathrm{Ma} = 85,\ \mathrm{Ca} = 0.0001$	−0.30730	0.24500
$L_1 = 0.5,\ L_2 = 0.01,\ k = 4,\ \mathrm{Ma} = 15,\ \mathrm{Ca} = 0.01$	−0.402385	−3.45082
$L_1 = 0.2,\ L_2 = 0.01,\ k = 4,\ \mathrm{Ma} = 45,\ \mathrm{Ca} = 0.01$	−0.695511	−3.47756

IV. SUMMARY

In this paper, we have carried out the linear stability analysis for the Marangoni instability in a linear Jeffreys viscoelastic fluid with a deformable liquid-gas interface in the gravity field subjected to a differential heating between an underlying uniform-temperature wall and the adjacent gas phase. The analysis has been performed with and without taking into account slippage at the wall and in the absence of buoyancy effects which is justified in the case of a thin layer. The fluid layer is assumed to be deposited on a solid substrate held at the constant temperature higher than that of the ambient gas phase. The surface tension of the fluid linearly decreases with the temperature introducing Marangoni stresses at the layer interface. The problem contains seven dimensionless parameters, namely the Biot, Bond, capillary, Prandtl, and Marangoni numbers, along with the dimensionless rheological relaxation and retardation numbers. The problem reduces naturally to that for a Newtonian fluid when the two latter parameters vanish.

The main findings of the present paper are now listed next. Our investigation reveals that the Marangoni stresses lead to two types of instability modes, namely (i) a stationary instability mode characterized by a growth rate expressed by a real (in general, complex) dominant eigenvalue $s = s_r + is_i$ with $s_i = 0$ and (ii) an oscillatory instability mode which manifests at the instability threshold via the emergence of two modes with complex conjugate purely imaginary dominant eigenvalues at the instability threshold which possess the same growth rate and propagate in opposite directions with the same speed.

We have found that stationary instability may be either long wave or short wave. The *genuine* long-wave ($k = 0$) regime of the stationary instability mode (or LW instability in short) is strongly affected by the interface deformability expressed by the value of Ca, whereas the SW instability with the wave number $k \sim 1$ range of the stationary mode disappears above a certain value of Ca depending on the values of other parameters. Similarly to other works [31,32] we have found codimension-two points of the system. However, unlike the codimension-two points in Refs. [31,32] representing intersection between both finite-wavelength stationary and oscillatory modes, in our case they represent coexistence of the LW stationary mode with either finite-wavelength stationary or oscillatory mode. We have also revealed, for the first time to the best of our knowledge, the existence of codimension-three points where LW, SW, and oscillatory modes coexist.

We emphasize that accounting for deformability of the free surface of the layer leads to revealing the emergence of the long-wave stationary Marangoni instability in the Jeffreys viscoelastic fluid in contradistinction to the previous theoretical studies [18–24] that considered nondeformable free surface, corresponding to $\mathrm{Ca} = 0$. The oscillatory modes of instability are all short wave and are moderately affected by Ca as compared to the long-wave instability. The critical Marangoni number for the oscillatory modes can be significantly reduced by either increasing the relaxation constant L_1 or decreasing the retardation constant L_2. At the same time, the instability threshold for the stationary mode is invariant with respect to variation in Pr, L_1, and L_2, similarly to its independence of the Prandtl number in the case of a Newtonian liquid. Our analysis shows the existence of a parametric regime where the oscillatory instability mode sets in first becoming unstable at a lower Ma than for the stationary mode, thereby showing the importance of accounting for (and not neglecting) the fluid viscoelasticity when present in the real system. The interface deformability plays a major role in selection of the dominant instability mode. Its increase favors the emergence of LW instability, thereby making it the dominant instability mode in a wider parameter domain as compared to the SW instability. The present study, therefore, demonstrates that even for a highly elastic fluid, the interface deformability triggers the LW instability to set in before the oscillatory instability.

An increase in Bi leads to an increase in the critical value of Ma_c for both stationary and oscillatory modes, thereby displacing the neutral stability curve toward higher values of Ma. A decrease in Bo, however, has a strong effect on the LW instability but a negligible effect on the SW instability and the oscillatory modes. In the presence of slippage at the substrate, an increase

in the value of the slip coefficient ζ leads to a moderate increase in Ma_c in the case of the stationary long-wave mode while the long-wave character of the instability is preserved. However, an increasing slippage leads to decrease in Ma_c and k_c for the SW mode. In the case of the oscillatory instability mode, variation in ζ results in a nonmonotonic variation in both the critical values of Ma_c and the wave number k_c.

As noted in the Introduction, only a few papers investigated Marangoni instability in a layer of a linear Jeffreys viscoelastic liquid with the deformable interface. The coupled Bénard-Marangoni instability was addressed based on the Boussinesq equations and the emergence of both finite-wavelength stationary and oscillatory modes of instability was identified [31,32]. Physical validity of these results was already discussed there and in the Introduction of this paper. Comparing between the contents of our paper and those of other relevant papers, we conclude that only the paper by Sarma and Mondal [33], where a pure Marangoni instability in a viscoelastic Maxwell liquid was studied, may be comparatively examined. In the case of a layer of a Jeffreys liquid with the deformable interface considered here, the Marangoni instability fed by a constant temperature of the solid substrate possesses long-wave stationary mode of instability with a *zero* wave number k_c along with both finite-wavelength (also referred to as short wave) stationary and oscillatory modes, whereas in the case of the Marangoni instability in a Maxwell liquid driven by a constant temperature gradient at the substrate [33], the instability modes were finite-wavelength oscillatory and long wave stationary and oscillatory with $0 < k_c \ll 1$. Also, in the case of Ref. [33], the instability was frequently set by competition between two oscillatory (long- and short-wave) modes; whereas in our case this scenario could be set by the long-wave stationary and finite-wavelength oscillatory modes but also by three modes via codimension-three point mentioned above.

The perturbation energy analysis reveals the dominant effect of the liquid elasticity and interfacial deformability on the emergence of the oscillatory instability. In the case of a Newtonian fluid, the surface stress work which is due to the presence of the Marangoni stress and the pressure work lead to the growth of the perturbation energy, whereas the bulk stress work leads only to viscous dissipation. The pressure work is nonzero in the present study due to the interface deformability and leads to an increase in the perturbation energy. However, in the case of a viscoelastic fluid, due to elastic relaxation, the bulk stress work also leads to an increase in the perturbation energy in contradistinction to a Newtonian fluid when oscillatory modes are involved. The energy increase due to the bulk stress work plays therefore a major role in the emergence of the oscillatory Marangoni instability in linear viscoelastic Jeffreys liquid.

The present study shows the dominance of the long-wave instability in certain parametric regimes where a thin-film analysis [1] should be applicable. It would be also important to investigate how the viscoelasticity of the fluid affects the type of bifurcation from the equilibrium exhibited by the system. Thus, a weakly nonlinear analysis would be the next step in understanding the effect of fluid viscoelasticity on the thermocapillary instability. Furthermore, from the applications' point of view, it would be important to reveal whether a thin viscoelastic film will rupture and whether this rupture can be prevented or controlled. Therefore, nonlinear analysis of the system dynamics may lead to a deeper understanding of the fluid viscoelasticity impact on the film dynamics subjected to the Marangoni effect. All of these are now underway and the results will be reported and discussed elsewhere.

ACKNOWLEDGMENTS

This research was supported by Grant No. 356/18 from the Israel Science Foundation (ISF). R.P. was partially supported by the Technion Funds Postdoctoral Fellowship. Y.A. was partially supported by the Millstone/St. Louis Chair in Civil and Environmental Engineering. A.O. was partially supported by the David T. Siegel Chair in Fluid Mechanics.

APPENDIX: DETAILS OF THE NUMERICAL APPROACH

To carry out the linear stability analysis of the problem at hand, the pseudospectral method is employed in which the eigenfunctions are expanded into series of the Chebyshev polynomials. For convenience, the domain $0 \leqslant z \leqslant 1$ is transformed into $-1 \leqslant z \leqslant 1$ by stretching $z \to 2z - 1$.

The eigenfunctions for the perturbed velocity, stresses, pressure, and temperature fields in Eqs. (12)–(14) are expanded in terms of the Chebyshev polynomials as

$$\tilde{v}_x(z) = \sum_{m=0}^{m=N} a_m T_m(z); \quad \tilde{v}_z(z) = \sum_{m=0}^{m=N} b_m T_m(z); \quad \tilde{p}(z) = \sum_{m=0}^{m=N} c_m T_m(z), \quad \tilde{\tau}_{xx}(z) = \sum_{m=0}^{m=N} d_m T_m(z);$$
$$\tilde{\tau}_{xz}(z) = \sum_{m=0}^{m=N} e_m T_m(z); \quad \tilde{\tau}_{zz}(z) = \sum_{m=0}^{m=N} f_m T_m(z), \quad \tilde{T}(z) = \sum_{m=0}^{m=N} g_m T_m(z), \tag{A1}$$

where $T_m(z)$ are Chebyshev polynomials of degree m and N is the highest degree of the polynomial in the series expansion or, equivalently, the number of collocation points. The coefficients a_m, b_m, c_m, d_m, e_m, f_m, and g_m are the unknowns to be solved for. The expansion series for the derivatives of the eigenfunctions is simply obtained by taking derivative of the series as, for instance,

$$D\tilde{v}_x(z) = \sum_{m=0}^{m=N} a_m DT_m(z), \tag{A2}$$

where $D = d/dz$ is the differentiation operator. Similar expansions are written for the rest of dependent variables in Eq. (A1) as well. All series expansions are then substituted into the governing equations to yield

$$ik \sum_{m=0}^{m=N} a_m T_m(z) + \sum_{m=0}^{m=N} b_m DT_m(z) = 0, \tag{A3a}$$

$$\frac{1}{\mathrm{Pr}} \sum_{m=0}^{m=N} a_m T_m(z) = -ik \sum_{m=0}^{m=N} c_m T_m(z) + ik \sum_{m=0}^{m=N} d_m T_m(z) + \sum_{m=0}^{m=N} e_m DT_m(z), \tag{A3b}$$

$$\frac{1}{\mathrm{Pr}} s \sum_{m=0}^{m=N} b_m T_m(z) = -\sum_{m=0}^{m=N} c_m DT_m(z) + ik \sum_{m=0}^{m=N} e_m T_m(z) + \sum_{m=0}^{m=N} f_m DT_m(z), \tag{A3c}$$

$$s \sum_{m=0}^{m=N} g_m T_m(z) - \sum_{m=0}^{m=N} b_m T_m(z) = \sum_{m=0}^{m=N} g_m D^2 T_m(z) - k^2 \sum_{m=0}^{m=N} g_m T_m(z), \tag{A3d}$$

$$(1 + L_1 s) \sum_{m=0}^{m=N} d_m T_m(z) = 2ik(1 + L_2 s) \sum_{m=0}^{m=N} a_m T_m(z), \tag{A4a}$$

$$(1 + L_1 s) \sum_{m=0}^{m=N} e_m T_m(z) = (1 + L_2 s) \left[\sum_{m=0}^{m=N} a_m DT_m(z) + ik \sum_{m=0}^{m=N} b_m T_m(z) \right], \tag{A4b}$$

$$(1 + L_1 s) \sum_{m=0}^{m=N} f_m T_m(z) = 2(1 + L_2 s) \sum_{m=0}^{m=N} b_m DT_m(z). \tag{A4c}$$

The boundary conditions (14a) at the solid substrate, i.e., $z = -1$, become

$$\sum_{m=0}^{m=N} a_m T_m(-1) = 0; \quad \sum_{m=0}^{m=N} b_m T_m(-1) = 0; \quad \sum_{m=0}^{m=N} g_m T_m(-1) = 0. \tag{A5}$$

There are four boundary conditions at the free surface, one of which is utilized to eliminate the amplitude of the perturbed location of the free surface $\tilde{\xi}$. Here the normal stress balance boundary condition (14d) is solved for ξ, which yields an expression of $\tilde{\xi}$ in terms of the perturbed pressure and normal stress component

$$\tilde{\xi} = -\frac{\mathrm{Ca}}{\mathrm{Bo} + k^2}(-\tilde{p} + \tilde{\tau}_{zz}). \tag{A6}$$

Equation (A6) is then substituted into the rest of the boundary conditions. The kinematic boundary condition now yields

$$\tilde{v}_x + s\frac{\mathrm{Ca}}{\mathrm{Bo} + k^2}(-\tilde{p} + \tilde{\tau}_{zz}) = 0 \tag{A7}$$

and substitution of the Chebyshev series expansion into it results in

$$\sum_{m=0}^{m=N} a_m T_m(1) + s\frac{\mathrm{Ca}}{\mathrm{Bo} + k^2}\left[-\sum_{m=0}^{m=N} c_m T_m(1) + \sum_{m=0}^{m=N} f_m T_m(1) \right] = 0. \tag{A8}$$

A similar procedure is then followed for the rest of the boundary conditions at the free surface $z = 1$.

The generalized eigenvalue problem is then constructed in the form

$$\mathbf{Ae} + s\mathbf{Be} = 0, \tag{A9}$$

where **A** and **B** are the matrices obtained from the discretization procedure explained above and **e** is the vector containing the coefficients of all series expansions (A1).

In these matrices, each eigenfunction corresponds to an $N \times N$ block, so $\tilde{v}_x$ occupies the first N rows and columns, the second eigenfunction $\tilde{v}_z$ occupies the next N rows and columns from the $N + 1$ to $2N$, and so on. Thus, matrices **A** and **B** are of order $7N \times 7N$.

Now, in order to incorporate the boundary conditions into the discretized matrices the following procedure is employed: For the boundary conditions at $z = -1$, the Nth row in the expansion for $\tilde{v}_x$ is replaced by the first boundary condition of Eq. (A5). Similarly, to impose the second boundary condition of Eq. (A5) for $\tilde{v}_z$, the $2N$th row is replaced in a similar way. A similar procedure is then applied toward the temperature boundary condition via the $7N$th row.

As for the boundary conditions at the free surface at $z = 1$, to impose the kinematic boundary condition, the first row for $\tilde{v}_x$ is replaced by Eq. (A8). The contributions of the pressure and normal stress terms will appear between the $(2N + 1)$th column to the $(3N)$th and between the $(5N + 1)$th column to the $(6N)$th. A similar procedure is then implemented for the rest of the boundary conditions at the free surface.

Further details of the discretization of the governing equations and boundary conditions, and of the construction of the matrices **A** and **B**, can be found in the standard procedure described by Trefethen [45] and Schmid and Henningson [46]. Next, we use the *polyeig* MATLAB routine to solve the constructed generalized eigenvalue problem Eq. (A9). To filter out the spurious modes from the numerically computed spectrum of the problem, the latter is obtained for N and $N + 2$ collocation points, and the eigenvalues are compared with a specified tolerance, e.g., 10^{-4}. The genuine eigenvalues are verified by increasing the number of collocation points by 25 and monitoring the variation of the obtained eigenvalues. Whenever the eigenvalue does not change to a prescribed precision, e.g., to the sixth significant digit, the same number of collocation points is used to determine the critical parameters of the system. In the present work, $N = 50$ is found to be sufficient to achieve the convergence and to determine the leading most unstable eigenvalue within the investigated parameter range.

[1] A. Oron, S. H. Davis, and S. G. Bankoff, Long-scale evolution of thin liquid films, Rev. Mod. Phys. **69**, 931 (1997).
[2] R. V. Craster and O. K. Matar, Dynamics and stability of thin liquid films, Rev. Mod. Phys. **81**, 1131 (2009).
[3] R. Mukherjee and A. Sharma, Instability, self-organization and pattern formation in thin soft films, Soft Matter **11**, 8717 (2015).
[4] J. P. Singer, Thermocapillary approaches to the deliberate patterning of polymers, J. Polym. Sci. Part B: Polym. Phys. **55**, 1649 (2017).
[5] S. H. Davis, Thermocapillary instabilities, Annu. Rev. Fluid Mech. **19**, 403 (1987).
[6] M. F. Schatz and G. P. Neitzel, Experiments on thermocapillary instabilities, Annu. Rev. Fluid Mech. **33**, 93 (2001).
[7] J. R. A. Pearson, On convection cells induced by surface tension, J. Fluid Mech. **4**, 489 (1958).
[8] H. Bénard, Les tourbillons cellulaires dans une nappe liquide transportant de la chaleur par convection en régime permanent, Ann. Chim. Phys. **23**, 62 (1901).
[9] L. E. Scriven and C. V. Sternling, On cellular convection driven by surface-tension gradients, effects of mean surface tension and surface viscosity, J. Fluid Mech. **19**, 321 (1964).
[10] K. A. Smith, On convective instability induced by surface-tension gradients, J. Fluid Mech. **24**, 401 (1966).
[11] S. H. Davis and G. M. Homsy, Energy stability theory for free-surface problems: Buoyancy-thermocapillary layers, J. Fluid Mech. **98**, 527 (1980).
[12] S. Shklyaev, M. Khenner, and A. A. Alabuzhev, Oscillatory and monotonic modes of long-wave Marangoni convection in a thin film, Phys. Rev. E **82**, 025302 (2010).
[13] S. Shklyaev, M. Khenner, and A. A. Alabuzhev, Long-wave Marangoni convection in a thin film heated from below, Phys. Rev. E **85**, 016328 (2012).
[14] A. E. Samoilova and N. I. Lobov, On the oscillatory Marangoni instability in a thin film heated from below, Phys. Fluids **26**, 064101 (2014).
[15] R. B. Bird, R. C. Armstrong, and O. Hassager, *Dynamics of Polymeric Liquids. Vol. 1: Fluid Mechanics* (Wiley Interscience, New York, 1987).
[16] R. R. Huilgol and N. Phan-Thien, *Fluid Mechanics of Viscoelasticity: General Principles, Constitutive Modelling, Analytical and Numerical Techniques* (Elsevier, Amsterdam, 1997).
[17] R. Blossey, *Thin Liquid Films: Dewetting and Polymer Flow* (Springer Science & Business Media, New York, 2012).
[18] D. Getachew and S. Rosenblat, Thermocapillary instability of a viscoelastic liquid layer, Acta Mech. **55**, 137 (1985).
[19] G. Lebon, P. Parmentier, O. Teller, and P. Dauby, Bénard-Marangoni instability in a viscoelastic Jeffreys' fluid layer, Rheol. Acta **33**, 257 (1994).
[20] G. Lebon and A. Cloot, An extended thermodynamic approach to non-Newtonian fluids and related results in Marangoni instability problem, J. Non-Newt. Fluid Mech. **28**, 61 (1988).
[21] P. C. Dauby, P. Parmentier, G. Lebon, and M. Gimela, Coupled buoyancy and thermocapillary convection in a viscoelastic Maxwell fluid, J. Phys.: Condens. Matter **5**, 4343 (1993).
[22] P. G. Siddheshwar, G. N. Sekhar, and G. Jayalatha, Surface tension driven convection in viscoelastic liquids with thermorheological effect, Int. Commun. Heat Mass Transfer **38**, 468 (2011).
[23] I. J. Hernandez Hernandez and L. A. Davalos-Orozco, Competition between stationary and oscillatory viscoelastic thermocapillary convection of a film coating a thick wall, Int. J. Thermal Sci. **89**, 164 (2015).
[24] S. D. R. Wilson, Growth rates of the Marangoni instability in a layer of elastic liquid, Rheol. Acta **34**, 601 (1995).
[25] M. Li, S. Xu, and E. Kumacheva, Convection in polymeric fluids subjected to vertical temperature gradients, Macromolecules **33**, 4972 (2000).
[26] F. Du, J. R. Felts, X. Xie, J. Z. Song, Y. H. Li, M. R. Rosenberger, A. E. Islam, S. H. Jin, S. N. Dunham, C. X. Zhang, W. L. Wilson, Y. G. Huang, W. P. King, and J. A. Rogers, Laser-induced nanoscale thermocapillary flow for purification of aligned arrays of single-walled carbon nanotubes, ACS Nano **8**, 12641 (2014).

[27] G. S. Jeong, J. L. Da Yoon No, J. Yoon, S. Chung, and S.-H. Lee, Viscoelastic lithography for fabricating self-organizing soft micro-honeycomb structures with ultra-high aspect ratios, Nat. Commun. **7**, 11269 (2016).
[28] E. L. Koschmieder and M. I. Biggerstaff, Onset of surface-tension-driven Bénard convection, J. Fluid Mech. **167**, 49 (1986).
[29] E. L. Koschmieder and D. W. Switzer, The wavenumbers of supercritical surface-tension-driven Bénard convection, J. Fluid Mech. **240**, 533 (1992).
[30] K. T. Chiang, Dealing with complicated starting value shooting process with Broyden's method: Example of the onset of convection for the viscoelastic fluid, Int. Commun. Heat Mass Transfer **31**, 815 (2004).
[31] H. Ramkissoon, G. Ramdath, D. Comissiong, and K. Rahaman, On thermal instabilities in a viscoelastic fluid, Int. J. Nonlinear Mech. **41**, 18 (2006).
[32] D. M. G. Comissiong, T. D. Dass, H. Ramkissoon, and A. R. Sankar, On thermal instabilities in a viscoelastic fluid subject to internal heat generation, Int. J. Math. Phys. Elect. Comput. Sci. **5**, 1152 (2011).
[33] R. Sarma and P. K. Mondal, Marangoni instability in a heated viscoelastic liquid film: Long-wave versus short-wave perturbations, Phys. Rev. E **100**, 013103 (2019).
[34] M. G. Velarde, A. A. Nepomnyashchy, and M. Hennenberg, Onset of oscillatory interfacial instability and wave motions in Bénard layers, Adv. Appl. Mech. **37**, 167 (2000).
[35] R. D. Benguria and M. C. Depassier, Oscillatory instabilities in the Rayleigh-Bénard problem with a free surface, Phys. Fluids **30**, 1678 (1987).
[36] C. Pérez-Garcia and G. Carneiro, Linear stability analysis of Bénard-Marangoni convection in fluids with a deformable free surface, Phys. Fluids A: Fluid Dyn. **3**, 292 (1991).
[37] D. V. Lyubimov, T. P. Lyubimova, N. I. Lobov, and J. I. D. Alexander, Rayleigh-Bénard-Marangoni convection in a weakly non-Boussinesq fluid layer with a deformable surface, Phys. Fluids **30**, 024103 (2018).
[38] S. J. Bolanos and B. Vernescu, Derivation of the Navier slip and slip length for viscous flows over a rough boundary, Phys. Fluids **29**, 057103 (2017).
[39] H. J. Wilson, M. Renardy, and Y. Renardy, Structure of the spectrum in zero Reynolds number shear flow of the UCM and Oldroyd-B liquids, J. Non-Newtonian Fluid Mech. **80**, 251 (1999).
[40] M. D. Graham, Effect of axial flow on viscoelastic Taylor-Couette instability, J. Fluid Mech. **360**, 341 (1998).
[41] M. B. Peirotti, J. A. Deiber, J. A. Ressia, M. A. Villar, and E. M. Valles, Relaxation modes of molten polydimethylsiloxane, Rheol. Acta **37**, 449 (1998).
[42] K. N. Kowal, S. H. Davis, and P. W. Voorhees, Thermocapillary instabilities in a horizontal liquid layer under partial basal slip, J. Fluid Mech. **855**, 839 (2018).
[43] K. X. Hu, M. He, and Q. S. Chen, Instability of thermocapillary liquid layers for Oldroyd-B fluid, Phys. Fluids **28**, 033105 (2016).
[44] K. X. Hu, J. Peng, and K. Q. Zhu, The linear stability of plane Poiseuille flow of Burgers fluid at very low Reynolds numbers, J. Non-Newtonian Fluid Mech. **167-168**, 87 (2012).
[45] L. N. Trefethen, *Spectral Methods in MATLAB* (SIAM, Philadelphia, 2000).
[46] P. J. Schmid and D. S. Henningson, *Stability and Transition in Shear Flows* (Springer, New York 2001).